Ancestral mitochondrial apparatus derived from the bacterial type II secretion system

Lenka Horváthová[1*], Vojtěch Žárský[1*], Tomáš Pánek[2*$], Romain Derelle[3], Jan Pyrih[4], Alžběta Motyčková[1], Veronika Klápšťová[1], Martina Vinopalová[1], Lenka Marková[1], Luboš Voleman[1], Vladimír Klimeš[2], Markéta Petrů[1], Zuzana Vaitová[1], Ivan Čepička[5], Klára Hryzáková[6], Karel Harant[7], Michael W. Gray[8], Mohamed Chami[9], Ingrid Guilvout[10], Olivera Francetic[10], B. Franz Lang[11], Čestmír Vlček[12], Anastasios D. Tsaousis[4], Marek Eliáš[2#], Pavel Doležal[1#]

[1]Department of Parasitology, Faculty of Science, Charles University, BIOCEV, Průmyslová 595, Vestec, 252 42, Czech Republic
[2]Department of Biology and Ecology, Faculty of Science, University of Ostrava, Chittussiho 10, 710 00 Ostrava, Czech Republic
[3]School of Biosciences, University of Birmingham, Edgbaston, B15 2TT, UK
[4]Laboratory of Molecular & Evolutionary Parasitology, RAPID group, School of Biosciences, University of Kent, Canterbury, CT2 7NZ, UK
[5]Department of Zoology, Faculty of Science, Charles University, Viničná 7, Prague 2, 128 44, Czech Republic
[6]Department of Genetics and Microbiology, Faculty of Science, Charles University, Viničná 7, Prague 2, 128 44, Czech Republic[7]Proteomic core facility, Faculty of Science, Charles University, BIOCEV, Průmyslová 595, Vestec, 252 42, Czech Republic
[8]Department of Biochemistry and Molecular Biology and Centre for Comparative Genomics and Evolutionary Bioinformatics, Dalhousie University, Halifax, NS B3H 4R2, Canada
[9]Center for Cellular Imaging and NanoAnalytics, University of Basel, Mattenstrasse 26, CH-4058 Basel, Switzerland
[10]Institut Pasteur, Biochemistry of Macromolecular Interactions Unit, Department of Structural Biology and Chemistry, CNRS UMR3528, 75015 Paris, France
[11]Robert Cedergren Centre for Bioinformatics and Genomics, Département de Biochimie, Université de Montréal, Montreal, QC, Canada H3T 1J4
[12]Institute of Molecular Genetics, Czech Academy of Sciences, 142 20 Prague 4, Czech Republic
[$]Current address: Department of Zoology, Faculty of Science, Charles University, Viničná 7, Prague 2, 128 44, Czech Republic

*these authors equally contributed to the study
#corresponding authors: Marek Eliáš (marek.elias@osu.cz), Pavel Doležal (pavel.dolezal@natur.cuni.cz)

Abstract

The type 2 secretion system (T2SS) is present in some Gram-negative eubacteria and used to secrete proteins across the outer membrane. Here we report that certain representative heteroloboseans, jakobids, malawimonads and hemimastigotes unexpectedly possess homologues of core T2SS components. We show that at least some of them are present in mitochondria, and their behaviour in biochemical assays is consistent with the presence of a mitochondrial T2SS-derived system (miT2SS). We additionally identified 23 protein families co-occurring with miT2SS in eukaryotes. Seven of these proteins could be directly linked to the core miT2SS by functional data and/or sequence features, whereas others may represent different parts of a broader functional pathway, possibly also involving the peroxisome. Its distribution in eukaryotes and phylogenetic evidence together indicate that the miT2SS-centred pathway is an ancestral eukaryotic trait. Our findings thus have direct implications for the functional properties of the early mitochondrion.

Introduction

Mitochondria of all eukaryotes arose from the same Alphaproteobacteria-related endosymbiotic bacterium[1,2]. New functions have been incorporated into the bacterial blueprint during mitochondrial evolution, while many ancestral traits have been lost. Importantly, in some cases, these losses occurred independently in different lineages of eukaryotes, resulting in a patchy distribution of the respective ancestral mitochondrial traits in extant eukaryotes. Examples are the ancestral mitochondrial division apparatus (including homologues of bacterial Min proteins), the aerobic-type rubrerythrin system, or the tmRNA-SmpB complex, each retained in different subsets of distantly related protist lineages[3–5]. It is likely that additional pieces of the ancestral bacterial cell physiology will be discovered in mitochondria of poorly studied eukaryotes.

An apparent significant difference between the mitochondrion and bacteria (including those living as endosymbionts of eukaryotes) lies in the directionality of protein transport across their envelope. All bacteria export specific proteins from the cell via the plasma membrane using the Sec or Tat machineries[6], and many diderm (Gram-negative) bacteria exhibit specialized systems mediating further protein translocation across the outer membrane (OM)[7]. In contrast, the mitochondrion depends on a newly evolved protein import system spanning both envelope membranes and enabling import of proteins encoded by the nuclear genome[8]. The capacity of mitochondria to secrete proteins seems to be limited. Mitochondrial homologues of Tat translocase subunits occur in some eukaryotic taxa, but their role in protein secretion has not been established[9,10]. A mitochondrial homologue of the SecY protein (a Sec translocase subunit) has been described only in jakobids[11,12] and its function remains elusive[13]. No dedicated machinery for protein export from the mitochondrion across the outer mitochondrial membrane has been described.

One of the best characterized bacterial protein translocation machineries is the so-called type 2 secretion system (T2SS)[14,15]. The T2SS belongs to a large bacterial superfamily of type 4 pili (T4P)-related molecular machines, most of which secrete long extracellular filaments (pili) for motility, adhesion, or DNA uptake[16–18]. The T2SS constitutes a specialized secretion apparatus, whose filament (pseudopilus) remains in the

93 periplasm[14,15]. It is composed of 12-15 conserved components, commonly referred to as
94 general secretion pathway (Gsp) proteins, which assemble into four main subcomplexes
95 (Fig. 1A). The OM pore is formed by an oligomer of 15-16 molecules of the GspD
96 protein[19,20]. The subcomplex in the inner membrane (IM) is called the assembly platform
97 and consists of the central polytopic membrane protein GspF surrounded by single-pass
98 membrane proteins GspC, GspL, and GspM[21]. GspC links the assembly platform to the
99 OM pore by interacting with the periplasmic N-terminal domain of GspD[22,23]. The third
100 subcomplex, called the pseudopilus, is a helical filament formed mainly of GspG
101 subunits, with minor pseudopilins (GspH, GspI, GspJ and GspK) assembled at its tip[24].
102 Pseudopilus assembly from its inner membrane base is believed to push the periplasmic
103 T2SS substrate through the OM pore. The energy for pseudopilus assembly is provided
104 by the fourth subcomplex, the hexameric ATPase GspE, interacting with the assembly
105 platform from the cytoplasmic side[25,26]. Substrates for T2SS-mediated secretion are first
106 transported by the Tat (as folded proteins) or the Sec (in an unfolded form) system across
107 the IM into the periplasm, where they undergo maturation and/or folding. The folded
108 substrates are finally loaded onto the pseudopilus for the release outside the cell via the
109 OM pore. The known T2SS substrates differ among taxa and share no common sequence
110 or structural features. Proteins transported by the T2SS in different species include
111 catabolic enzymes (such as lipases, proteases or phosphatases) and, in the case of
112 bacterial pathogens, toxins[14]. A recent survey of bacterial genomes showed that the T2SS
113 is mainly present in Proteobacteria[18]. Crucially, neither the T2SS nor other systems of the
114 T4P superfamily have been reported from eukaryotes[7,14,18].
115 Here we show that certain distantly related eukaryotes unexpectedly contain
116 homologues of key T2SS subunits representing all four functional T2SS subcomplexes.
117 We provide evidence for mitochondrial localization of some of these eukaryotic Gsp
118 protein homologues and describe experimental results supporting the idea that they
119 constitute a system similar to the bacterial T2SS. Furthermore, we point to the existence
120 of 23 proteins with a perfect taxonomic co-occurrence with the eukaryotic Gsp
121 homologues. Some of these co-occurring proteins seem to be additional components of
122 the mitochondrial T2SS-related machinery, whereas others are candidates for components
123 of a broader functional pathway linking the mitochondrion with other parts of the cell.
124 Given its phylogenetic distribution, we propose that the newly discovered pathway was
125 ancestrally present in eukaryotes. Its further characterization may provide fundamental
126 new insights into the evolutionary conversion of the protomitochondrion into the
127 mitochondrial organelle.
128
129 **Results**
130 ***Certain protist lineages code for a conserved set of homologues of T2SS core***
131 ***components***
132 While searching the genome of the heterolobosean *Naegleria gruberi* for proteins of
133 bacterial origin with a possible mitochondrial role, we surprisingly discovered
134 homologues of four core subunits of the bacterial T2SS, specifically GspD, GspE, GspF,
135 and GspG (Fig. 1A; Supplementary Table 1). Using genomic and transcriptomic data
136 from public repositories and our on-going sequencing projects for several protist species
137 of key evolutionary interest (see Methods), we mapped the distribution of these four
138 components in eukaryotes. All four genes were found in the following characteristic set

139 of taxa (Fig. 1B, Supplementary Table 1): three additional heteroloboseans (*Naegleria*
140 *fowleri*, *Neovahlkampfia damariscottae*, *Pharyngomonas kirbyi*), two jakobids (*R.*
141 *americana* and *Andalucia godoyi*), and two malawimonads (*Malawimonas jakobiformis*
142 and *Gefionella okellyi*). In addition, single-cell transcriptomes from two species of
143 Hemimastigophora (hemimastigotes[27]) revealed the presence of homologues of GspD and
144 GspG (*Hemimastix kukwesjijk*) and GspG only (*Spironema* cf. *mulitciliatum*), possibly
145 reflecting incompleteness of the data. Finally, three separate representatives of the
146 heterolobosean genus *Percolomonas* (Supplementary Fig. 1) each exhibited a homologue
147 of GspD, but not of the remaining Gsp proteins, in the available transcriptomic data. In
148 contrast, all four genes were missing in sequence data from all other eukaryotes
149 investigated, including the genome and transcriptome of another malawimonad
150 ("Malawimonas californiana") and deeply-sequenced transcriptomes of a third jakobid
151 (*Stygiella incarcerata*) and four additional heteroloboseans (*Creneis carolina*,
152 *Dactylomonas venusta*, *Harpagon schusteri*, and the undescribed strain Heterolobosea sp.
153 BB2).
154 Probing *N. gruberi* nuclei with fluorescence *in situ* hybridization ruled out an
155 unidentified bacterial endosymbiont as the source of the *Gsp* genes (Supplementary Fig.
156 2). Moreover, the eukaryotic *Gsp* genes usually have introns and constitute robustly
157 supported monophyletic groups well separated from bacterial homologues (Fig. 2;
158 Supplementary Fig. 3), ruling out bacterial contamination in all cases. In an attempt to
159 illuminate the origin of the eukaryotic Gsp proteins we carried out systematic
160 phylogenetic analyses based on progressively expanded datasets of prokaryotic
161 homologues and for each tree inferred the taxonomic identity of the bacterial ancestor of
162 the eukaryotic branch (see Methods for details on the procedure). The results,
163 summarized in Supplementary Fig. 3, showed that the inference is highly unstable
164 depending on the dataset analysed, and no specific bacterial group can be identified as an
165 obvious donor of the eukaryotic Gsp genes. This result probably stems from a
166 combination of factors, including the long branches separating the eukaryotic and
167 bacterial Gsp sequences, the length of Gsp proteins restricting the amount of the
168 phylogenetic signal retained, and perhaps also rampant horizontal gene transfer (HGT) of
169 the T2SS system genes between bacterial taxa. The eukaryotic Gsp genes are in fact so
170 divergent that some of them could not be unambiguously classified as specific
171 homologues of T2SS components (rather than the related machineries of the T4P
172 superfamily) when analysed using models developed for the bacterial genomes[18]
173 (Supplementary Fig. 3).
174 Heteroloboseans, jakobids and malawimonads have been classified in the
175 supergroup Excavata[28]. However, recent phylogenomic analyses indicate that excavates
176 are non-monophyletic and even suggest that malawimonads are separated from
177 heteroloboseans and jakobids by the root of the eukaryote phylogeny[29–32]. Together with
178 the presence of at least some Gsp proteins in hemimastigotes, which constitute an
179 independent eukaryotic supergroup[27], it is likely that the T2SS-related proteins were
180 present in the last eukaryotic common ancestor (LECA) but lost in most eukaryote
181 lineages (Fig. 1B). Heteroloboseans and malawimonads have two GspG paralogues, but
182 the phylogenetic analyses did not resolve whether this is due to multiple independent
183 GspG gene duplications or one ancestral eukaryotic duplication followed by loss of one
184 of the paralogues in jakobids (Fig. 2; Supplementary Fig. 3D; Supplementary Table 1).

185
186 ***The eukaryotic Gsp proteins localize to the mitochondrion***
187 We hypothesized that the eukaryotic homologues of the four Gsp proteins are parts of a
188 functional T2SS-related system localized to the mitochondrion. This notion was
189 supported by the presence of predicted N-terminal mitochondrial targeting sequences
190 (MTSs) in some of the eukaryotic Gsp proteins (Supplementary Table 1). The prediction
191 algorithms identified putative N-terminal MTSs for proteins from jakobids and
192 malawimonads but failed to recognize them in the orthologues from heteroloboseans,
193 which, however, carry the longest N-terminal extensions (Supplementary Fig. 4).
194 In order to test if Gsp proteins carry functional mitochondrial targeting
195 information, we expressed *GspD*, *GspE* and *GspG1* genes from *N. gruberi* (*Ng*) and *G.*
196 *okellyi* (*Go*) in *Saccharomyces cerevisiae*; no expression of *GspF* was achieved. All
197 proteins were specifically localised in mitochondria, as confirmed by their co-localisation
198 with Mitotracker red CMX Ros (Fig. 3A). Additionally, we attempted to express these
199 genes in *Trypanosoma brucei*, which represents the evolutionarily closest experimental
200 model to the eukaryotes carrying the *Gsp* genes. Of all the proteins tested, only *Go*GspD
201 and *Go*GspG2 were detected (Fig. 3B), in addition to a weak signal for *Ng*GspG1
202 (Supplementary Fig. 5A). While both GspG proteins could be found specifically in the
203 mitochondrion of *T. brucei*, *Go*GspD was found in a different membrane compartment,
204 perhaps due to mistargeting. Finally, we tested if the atypically long N-terminal extension
205 of *Ng*GspG1 targets the protein to the *T. brucei* mitochondrion. Indeed, the 160 N-
206 terminal amino acid residues of *Ng*GspG1 were able to deliver the marker (mNeonGreen)
207 into the organelle (Supplementary Fig. 5B). As a complementary approach, we raised
208 specific polyclonal antibodies against *Ng*GspG1 and probed *N. gruberi* cellular fractions
209 (Fig. 3C; Supplementary Fig. 6). *Ng*GspG1 and *Ng*GspEN2A co-fractionated with the
210 mitochondrial markers including alternative oxidase (AOX) and TatC[9], but not with the
211 cytosolic protein hemerythrin[33]. Immunofluorescence microscopy of *N. gruberi* with the
212 anti-*Ng*GspG1 antibody provided further evidence that *Ng*GspG1 is targeted to
213 mitochondria (Fig. 3D, Supplementary Fig. 7).
214 In order to further confirm the mitochondrial localization of the Gsp proteins in *N.*
215 *gruberi*, we analysed the mitochondrial proteome of this organism by partial purification
216 of the organelle and identification of resident proteins by mass spectrometry. A
217 mitochondria-enriched fraction was obtained from a cellular lysate by several steps of
218 differential centrifugation and OptiPrep gradient centrifugation. Three sub-fractions of
219 different densities, named accordingly as Opt1015, Opt1520, Opt2030, were collected
220 (Supplementary Fig. 8A, see Methods for more details), with the densest one being most
221 enriched in mitochondria. The sub-fractions were subjected to proteomic analysis. The
222 relative amount of each protein in each sub-fraction was determined by label-free
223 quantification and the proteins were grouped by a multicomponent analysis (for details
224 see Methods) according to their distributions across the gradient (Fig. 3E). A set of
225 marker proteins (homologues of well-characterized typical mitochondrial proteins from
226 other species) was used to identify a cluster of mitochondrial proteins. Due to the partial
227 co-purification of peroxisomes with mitochondria, a peroxisome-specific cluster was
228 defined analogously. As a result, 946 putative mitochondrial and 78 putative peroxisomal
229 proteins were identified among the total of 4,198 proteins detected in all three sub-
230 fractions combined. Encouragingly, the putative mitochondrial proteome of *N. gruberi* is

231 dominated by proteins expected to be mitochondrial or whose mitochondrial localization
232 is not unlikely (Supplementary Fig. 8B, Supplementary Table 2A). On the other hand, the
233 putative peroxisomal proteome seems to be contaminated by mitochondrial proteins
234 (owing to the presence of several mitochondrial ribosomal proteins; Supplementary Table
235 2B). Importantly, all five Gsp proteins (including both GspG paralogues) were identified
236 in the putative mitochondrial but not peroxisomal proteome of *N. gruberi*.
237
238 ***The properties of the eukaryotic Gsp proteins support the existence of a mitochondrial***
239 ***T2SS-related machinery***
240 The foregoing experiments support the idea that all four eukaryotic Gsp homologues
241 localize to and function in the mitochondrion. However, direct *in vivo* demonstration of
242 the existence of a functional mitochondrial T2SS-related machinery is currently not
243 feasible, because none of the Gsp homologue-carrying eukaryotes represents a tractable
244 genetic system. We thus used *in vitro* approaches and heterologous expression systems to
245 test the key properties of the eukaryotic Gsp proteins.
246 Crucial for the T2SS function is the formation of the OM pore, which is a β-barrel
247 formed by the oligomerization of the C-domain of the GspD protein[34]. The actual
248 assembly of the bacterial pore requires GspD targeting to the outer membrane through
249 interaction of its very C-terminal domain (S-domain) with the outer membrane
250 lipoprotein GspS[35]. GspD forms a pre-pore multimer, whose OM membrane insertion is
251 independent on the β□barrel assembly machinery (BAM) complex[36,37]. In addition, the
252 bacterial GspD carries four short N-terminal domains exposed to the periplasm, called N0
253 to N3, of which N1 to N3 share a similar fold[38] (Fig. 4A). While the N3 domain is
254 required for the pore assembly[39], N0 interacts with GspC of the assembly platform[22,40].
255 Sequence analysis of the mitochondrial GspD homologue revealed that it corresponds to
256 a C-terminal part of the bacterial GspD C-domain, whereas the N-terminal domains N0 to
257 N3, the N-terminal part of the C-domain, and the S-domain are missing (Fig. 4A;
258 Supplementary Fig. 4A).
259 According to our hypothesis, the mitochondrial GspD should be present in the
260 outer mitochondrial membrane. In order to test this localization, *N. gruberi* GspD
261 (*Ng*GspD) was *in vitro* imported into yeast mitochondria. The import reaction was also
262 performed with the widely used synthetic substrate Su9-DHFR destined to mitochondrial
263 matrix, which is composed of 69 amino acid residues of F_o-ATPase subunit 9 from
264 *Neurospora crassa* fused to the mouse DHFR[41]. Both proteins accumulated in the
265 mitochondria in a time-dependent manner, but only the import of Su9-DHFR could be
266 inhibited by the addition of ionophores, which dissipate membrane potential ($\Delta\Psi$) (Fig.
267 4B). This result showed that the import of GspD is independent of $\Delta\Psi$, which is a typical
268 feature of mitochondrial outer membrane proteins. The key question was if the
269 mitochondrial GspD homologue has retained the ability to assemble into an oligomeric
270 pore-forming complex. This possibility was supported by homology modelling of GspD
271 from *G. okellyi* (*Go*GspD) using *Vibrio cholerae* GspD[42] as a template, which indicated
272 that the protein has the same predicted fold as the typical secretin C-domain. Remarkably,
273 the two transmembrane β-strands of *Go*GspD are separated by the highly conserved
274 amphipathic helical loop (AHL) (Fig. 4C) essential for secretin membrane insertion,
275 suggesting its capability to form a pentadecameric pore complex. Indeed, radioactively
276 labelled *Go*GspD assembled into a high-molecular-weight complex of around 200 kDa in

277 an *in vitro* bacterial translation system in the presence of lecithin liposomes (Fig. 4D).
278 The complex was resistant to 2M urea treatment, which would remove nonspecific
279 protein aggregates, and was still pelleted with the liposomes, suggesting that it was
280 inserted into the liposomes. These results showed that the mitochondrial GspD, despite
281 being significantly truncated when compared to its bacterial homologues, has retained the
282 major characteristics of bacterial secretins[43], including the capacity to form oligomers and
283 insert into membranes.
284 To test if the mitochondrial GspD forms *bona fide* pores in the membrane, we
285 aimed to produce His-tagged *Ng*GspD in *E. coli* and purify the membrane complexes for
286 the electrophysiology analysis. Inducing the production of this protein in the bacterial
287 cytoplasm was highly toxic (Fig. 5A). A similar phenomenon has been reported for
288 bacterial secretins, which form pores in the inner bacterial membrane[43]. While this
289 hampered protein production and purification, directing the GspD export to the periplasm
290 by fusing it to the N-terminal signal peptide of *E. coli* DsbA protein alleviated the
291 toxicity upon autoinduction. The His-*Ng*GspD variant was affinity-purified on a Ni-
292 column followed by size exclusion chromatography, during which two peaks of about
293 230 kDa and 125 kDa could be observed (Fig. 5B). The pore-forming activity of His-
294 *Ng*GspD purified from both protein peaks was demonstrated by conductivity
295 measurements in black lipid membranes composed of an *E. coli* polar lipid extract. The
296 channel recordings illustrated a very high stability of the inserted membrane pores (Fig.
297 5C). The amplitude histograms (Fig. 5D) suggested that the mitochondrial GspD can
298 form variable arrangements resulting in stable membrane pores of different sizes.
299 The secretion mechanism of the T2SS relies on the assembly of pseudopilus made
300 up of GspG subunits[44]. Comparison of the mitochondrial GspG with bacterial
301 homologues revealed important similarities as well as differences. These proteins share a
302 complete pseudopilin domain preceded by a transmembrane domain, but the
303 mitochondrial proteins are substantially longer due to extensions at both N- and C-termini
304 (Fig. 6A). The N-terminal extension likely serves as a MTS, but the origin and function
305 of the C-terminal extension (amounting to ~100 amino acid residues) is unclear, as it is
306 well conserved among the mitochondrial GspG but lacks discernible homologues even
307 when analysed by highly sensitive homology-detection methods (HMM-HMM
308 comparisons with HHpred[45] and protein modelling using the Phyre2 server[46]). Structural
309 modelling of the pseudopilin domain into the recently obtained cryo-EM reconstruction
310 of the PulG (=GspG) complex from *Klebsiella oxytoca*[47] revealed the presence of key
311 structural features in the mitochondrial GspG from *G. okellyi* (*Go*GspG1), supporting
312 possible formation of a pseudopilus (Fig. 6B).
313 To test this directly, we purified a recombinant pseudopilin domain of *Ng*GspG1
314 under native conditions, which showed a uniform size of 25 kDa corresponding to the
315 monomer (Fig. 7A). Possible protein-protein interaction of the purified pseudopilin
316 domain was tested by thermophoresis of an NT-647-labelled protein. The measurements
317 revealed specific self-interaction and plotting of the change in thermophoresis yielded a
318 K_d of 216 (±15.1) nM (Fig. 7B). Additionally, the interaction properties of GspG were
319 followed by the bacterial two-hybrid assay (BACTH). When produced in bacteria, the
320 mitochondrial *Go*GspG1 showed specific oligomerisation, typical of bacterial major
321 pseudopilins[48], supporting its *in vivo* propensity to form a pseudopilus (Fig. 7C). An
322 analogous BACTH assay of *N. gruberi* Gsp proteins also showed GspG1 self-interaction

323 (data not shown). In addition, *Go*GspG1 showed positive interaction with *Go*GspF,
324 consistent with the analogous interaction of bacterial GspG with the IM-embedded
325 GspF[48]. Moreover, the mitochondrial *Go*GspF and *Go*GspE each formed dimers in the
326 BACTH assay (Fig. 7C). These interactions are consistent with the hypothesized role of
327 both proteins as mitochondrial T2SS components, as GspF forms dimers within the IM
328 complex and GspE assembles into an active hexameric ATPase in the bacterial T2SS
329 system. Indeed, bacterial GspG and GspF also interact in the BACTH assay[48]. Tests of all
330 other possible interactions of *G. okellyi* Gsp proteins were negative.
331 The *in silico* analyses and experiments described above are consistent with the
332 hypothesized existence of a functional mitochondrial secretion machinery derived from
333 the bacterial T2SS. However, the mitochondrial subunits identified would assemble only
334 a minimalist version of the secretion system, reduced to the functional core of the four
335 subcomplexes of the bacterial T2SS, i.e. the luminal ATPase (GspE), the IM pseudopilus
336 assembly platform (GspF), the intermembrane space pseudopilus (GspG), and the OM
337 pore (truncated GspD). Despite using sensitive HMM-based searches, we did not detect
338 homologues of other conserved T2SS subunits in any of the eukaryotes possessing GspD
339 to GspG proteins. One of the missing subunits is GspC, which connects the assembly
340 platform with the N0 domain of GspD pore[22,23]. Thus, the absence of GspC in eukaryotes
341 correlates with the lack of the N0 domain in the eukaryotic GspD. Analogously, the
342 absence of the C-terminal S-domain in the mitochondrial GspD (Fig. 4A), known to be
343 missing also from some bacterial GspD proteins, rationalizes the lack of a eukaryotic
344 homologue of the bacterial OM component GspS that binds to GspD via the S-domain
345 during the pore assembly[35]. The apparent lack of a eukaryotic homologue of GspL, which
346 interacts via its cytosolic domain with the N1E domain of the bacterial GspE [49], may
347 similarly be explained by the fact that the eukaryotic GspE protein seems to be
348 homologous only to the C-terminal (CTE) domain of its bacterial counterpart and lacks
349 an equivalent of the N1E domain (Supplementary Fig. 4E). The mitochondrial system
350 also apparently lacks a homologue of GspO, a bifunctional enzyme that is essential for
351 GspG maturation. Despite this absence, eukaryotic GspG homologues have conserved all
352 the characteristic sequence features required for GspG maturation (the polar anchor and
353 the trans-membrane domain with a conserved glutamate residue at position +5 relative to
354 the processing site) (Fig. 6A, Supplementary Fig. 4J). Notably, all the *Ng*GspG1 and
355 *Ng*GspG2-derived peptides detected in our proteomic analysis come from the region of
356 the protein downstream of the conserved processing site (Fig. 6C), suggesting that
357 analogous maturation of the pseudopilin also occurs in mitochondria.
358
359 ***New putative components of the mitochondrial T2SS-based functional pathway***
360 ***identified by phylogenetic profiling***
361 Since none of the eukaryotes with the Gsp homologues is currently amenable to
362 functional studies, we tried to further illuminate the role of the mitochondrial T2SS
363 system using a comparative genomic approach. Specifically, we reasoned that possible
364 additional components of the machinery, as well as its actual substrate(s), might show the
365 same phylogenetic distribution as the originally identified four subunits. Using a
366 combination of an automated identification of candidate protein families and subsequent
367 manual scrutiny by exhaustive searches of available eukaryote sequence data (for details
368 of the procedure see Methods), we identified 23 proteins (more precisely, groups of

369 orthologues) that proved to exhibit the same phylogenetic distribution in eukaryotes as
370 the four core T2SS components. Specifically, all 23 proteins were represented in each of
371 the heterolobosean, jakobid, and malawimonad species possessing all four core Gsp
372 proteins, whereas only 17 proteins were identified in the incomplete transcriptomic data
373 of hemimastigotes and seven of them were found in the transcriptomic data from the
374 *Percolomonas* lineage that possesses only GspD (Fig. 1B; Supplementary Table 1).
375 Except for two presumably Gsp-positive jakobids represented by incomplete EST surveys
376 and a case of a likely contamination (Supplementary Table 3), no orthologues of any of
377 these proteins were found in any other eukaryote (including the Gsp-lacking members of
378 heteroloboseans, jakobids and malawimonads). The sequences of these 23 proteins were
379 analysed by various *in silico* approaches, including HHpred and Phyre2 to assess their
380 possible function (Fig. 8A).
381 These analyses revealed that seven of the families have a direct link to the T2SS
382 suggested by discerned homology to known T2SS components. One of them represents
383 an additional, more divergent homologue of the C-terminal part of the bacterial GspD.
384 Hence, the protein has been marked as GspDL (GspD-like). Three other families, referred
385 to as GspDN1 to GspDN3, proved to be homologous to the Secretin_N domain (Pfam
386 family PF03958), present in the bacterial GspD protein as domains N1, N2 and N3 (Fig.
387 4A). The N1-N3 array protrudes into the periplasm, where it oligomerizes to form three
388 stacked rings[20]. As mentioned above, the initially identified eukaryotic GspD homologues
389 lack the N-terminal region, suggesting that the gene was split into multiple parts in
390 eukaryotes. While GspDN1 corresponds to a full single N-domain, GspDN2 and GspDN3
391 relate only to its C-terminal and N-terminal halves, respectively (Fig. 4A; Supplementary
392 Fig. 4B-D). Unfortunately, high sequence divergence makes it impossible to identify
393 potential specific correspondence between the N1 to N3 domains of the bacterial GspD
394 and the eukaryotic GspDN1 to GspDN3 proteins. Importantly, a Y2H assay indicated that
395 the two separate polypeptides GspD and GspDN1 of *N. gruberi* may interact *in vivo* (Fig.
396 4E), perhaps forming a larger mitochondrial complex. In addition, we identified most of
397 the newly discovered GspD-related proteins (GspDL/N) in the *N. gruberi* mitochondrial
398 proteome (the exception being GspDN1, which was not detected in a sufficient number of
399 replicates to be included in the downstream analysis; Supplementary Table 2A).
400 The final three proteins linked to the T2SS based on their sequence features seem
401 to be evolutionarily derived from GspE. One, denoted GspEL (GspE-like) represents a
402 divergent homologue of the C1E (i.e. nucleotide-binding) domain of GspE, although with
403 some of the characteristic motifs (Walker A, Asp box, Walker B) abrogated
404 (Supplementary Fig. 4F), indicating the loss of the ATPase function. The other two
405 proteins, which we denote GspEN2A and GspEN2B, are suggested by HHpred to be
406 related to just the N2E domain of the bacterial GspE (Supplementary Fig.4G and 4H).
407 GspEN2A and GspEN2B were identified among *N. gruberi* mitochondrial proteins in the
408 proteomic analysis, whereas GspEL was found in the cluster of putative peroxisomal
409 proteins. Importantly, a polyclonal antibody raised against *Ng*GspEN2A confirmed the
410 mitochondrial localization of the protein (Fig. 3C, D; Supplementary Fig. 6, 7).
411 The remaining sixteen proteins co-occurring with the core eukaryotic T2SS
412 subunits, hereafter referred to as Gcp (Gsp-co-occurring proteins), were divided into three
413 categories. The first comprises four proteins that constitute novel paralogues within
414 broader common eukaryotic (super)families. Three of them (Gcp1 to Gcp3) belong to the

415 WD40 superfamily and seem to be most closely related to the peroxisomal protein import
416 co-receptor Pex7 (Supplementary Fig. 9). None of these proteins has any putative N-
417 terminal targeting sequence, but interestingly, the peroxisomal targeting signal 1 (PTS1)
418 could be predicted on most Gcp1 and some Gcp2 proteins (Supplementary Table 1).
419 However, these predictions are not fully consistent with the results of our proteomic
420 analysis: *Ng*Gcp1 was found among the mitochondrial proteins and *Ng*Gcp2 in the cluster
421 of putative peroxisomal proteins (Supplementary Table 2), but PTS1 is predicted to be
422 present in the *Ng*Gcp1 protein (Supplementary Table 1). The fourth Gcp protein (Gcp4)
423 is a novel paralogue of the ubiquitin-like superfamily, distinctly different from the
424 previously characterized members including ubiquitin, SUMO, NEDD8 and others
425 (Supplementary Fig. 10).
426 The second Gcp category comprises eleven proteins (Gcp5 to Gcp15) well
427 conserved at the sequence level among the Gsp-containing eukaryotes, yet lacking any
428 discernible homologues in other eukaryotes or in prokaryotes. Two of these proteins
429 (Gcp8, Gcp15) were not identified in the proteomic analysis of *N. gruberi*
430 (Supplementary Tables 1 and 2). Of those identified, several (Gcp5, Gcp6, Gcp13) were
431 found among the mitochondrial proteins, whereas some others (Gcp9, Gcp10, Gcp11)
432 clustered with peroxisomal markers. Specific localization of the three remaining proteins
433 (Gcp7, Gcp12, and Gcp14) could not be determined due to their presence at the
434 boundaries of the mitochondrial or peroxisomal clusters. No homology to other proteins
435 or domains could be discerned for the Gsp5 to Gsp15 proteins even when sensitive
436 homology-detection algorithms were employed. However, four of them are predicted as
437 single-pass membrane proteins, with the transmembrane segment in the N- (Gcp7,
438 Gcp11, Gcp15) or C-terminal (Gcp5) regions (Fig. 8A; Supplementary Fig. 11).
439 Interestingly, Gcp6 and Gcp12 proteins contain multiple absolutely conserved cysteine or
440 histidine residues (Fig. 8A, B; Supplementary Fig. 12). We were not able to determine
441 their localization in *N. gruberi* by microscopy, but we tested the localization of *Go*Gcp12
442 upon expression in *T. brucei*, where it co-localized with the mitochondrial tubules (Fig.
443 8C).
444 Gcp16 constitutes a category of its own, as it typifies a novel protein family
445 present also in bacteria of the PVC superphylum (Supplementary Fig. 13). Phylogenetic
446 analysis confirmed that the eukaryotic members of the family are of the same origin
447 (Supplementary Fig. 14). Gcp16 proteins are predicted to harbour two transmembrane
448 domains (Supplementary Fig. 13). Furthermore, HHpred searches suggested possible
449 homology of a region of the Gcp16 protein (upstream of the transmembrane domains) to
450 various metallopeptidases, although with inconclusive statistical support. However,
451 inspection of the HHpred alignments revealed that Gcp16 shares with these hits an
452 absolutely conserved motif HEXXH (Supplementary Fig. 13), which is the catalytic,
453 metal-binding motif of the zincin tribe of metallopeptidases[50]. Interestingly, close to the
454 HEXXH motif, Gcp16 possesses an absolutely conserved EXXA motif, which is
455 diagnostic of a zincin subgroup called gluzincins[50], further supporting the notion that
456 Gcp16 may function as a membrane-embedded peptidase. Most eukaryotic Gcp16
457 proteins exhibit an N-terminal extension compared to the bacterial homologues
458 (Supplementary Fig. 13), but only some of these extensions are recognized as putative
459 MTSs and the *N. gruberi* Gcp16 was not identified either in putative mitochondrial or
460 peroxisomal proteome.

461
462 **Discussion**
463 Our analyses revealed that a subset of species belonging to four eukaryotic lineages share
464 a set of at least 27 proteins (or families of orthologues) absent from other eukaryotes for
465 which genomic or transcriptomic data are currently available (Fig. 1B). At least eleven of
466 these proteins (the Gsp proteins) are evolutionarily related to components of the bacterial
467 T2SS, although seven of them are so divergent that their evolutionary connection to the
468 T2SS could be recognized only retrospectively after their identification based on their
469 characteristic phylogenetic profile. For the sixteen remaining proteins (Gcp1 to Gcp16)
470 no other obvious evolutionary or functional link to the T2SS is evident apart from the
471 same phyletic pattern as exhibited by the T2SS subunit homologues. Nevertheless,
472 similar phylogenetic profiles are generally a strong indication for proteins being parts of
473 the same functional system or pathway, and have enabled identification of new
474 components of different cellular structures or pathways (e.g. refs [51,52]). Is it, therefore,
475 possible that the 27 Gsp/Gcp proteins similarly belong to a single functional pathway?
476 The phylogenetic profile shared by the eukaryotic Gsp and Gcp proteins is not
477 trivial, as it implies independent gene losses in a specific set of multiple eukaryotic
478 branches (Fig. 1B). The likelihood of a chance emergence of the same taxonomic
479 distribution of these proteins is thus low. Nevertheless, false positives cannot be
480 completely excluded among the Gcp proteins and their list may be revised when a more
481 comprehensive sampling of eukaryote genomes or transcriptomes becomes available. It is
482 also possible that the currently inferred phylogenetic profile of some of the Gsp/Gcp
483 proteins is incomplete due to limited sampling of the actual gene repertoire of species
484 represented by transcriptome assemblies only. The inherently incomplete nature of
485 single-cell transcriptome assemblies available for hemimastigotes potentially explains our
486 failure to identify homologues of some Gsp and Gcp proteins in this group (Fig. 1B;
487 Supplementary Table 1). An incomplete set is evident also in the heterolobosean
488 *Percolomonas* lineage, as transcriptomic data from three different members revealed only
489 the presence of GspD, GspDL, the three GspDN proteins, and four Gcp proteins (Fig. 1B,
490 Supplementary Table 1). The relatively coherent pattern of Gsp/Gcp protein occurrence
491 in the three independently sequenced transcriptomes and the fact that in other Gsp/Gcp-
492 containing eukaryotes (except for hemimastigotes) all 27 families are always represented
493 in the respective transcriptome assembly (Supplementary Table 1) suggest that the
494 *Percolomonas* lineage has indeed preserved only a subset of Gsp/Gcp families. Genome
495 sequencing is required to test this possibility.
496 All uncertainties notwithstanding, our data favour the idea that a hitherto
497 unrecognized complex functional pathway exists in some eukaryotic cells, underpinned
498 by most, if not all, of the 27 Gsp/Gcp proteins and possibly others yet to be discovered.
499 Direct biochemical and cell biological investigations are required for testing its existence
500 and the actual cellular role. Nevertheless, we have integrated the experimental data
501 gathered so far with the insights from bioinformatic analyses to propose a hypothetical
502 working model (Fig. 9).
503 Our main proposition is that the eukaryotic homologues of the bacterial Gsp
504 proteins assemble a functional transport system, here denoted miT2SS, that spans the
505 mitochondrial OM and mediates the export of specific substrate proteins from the
506 mitochondrion. Although the actual architecture of the miT2SS needs to be determined,

507 the available data suggest that it departs in detail from the canonical bacterial T2SS
508 organization, as homologues of some of the important bacterial T2SS components are
509 apparently missing. Most notable is the absence of GspC, presumably related to the
510 modified structure of its interacting partner GspD, which in eukaryotes is split into
511 multiple polypeptides and seems to completely lack the N0 domain involved in GspC
512 binding. It thus remains unclear whether and how the IM assembly platform and the OM
513 pore interact in mitochondria. One possible explanation is that GspC has been replaced
514 by an unrelated protein. It is notable that three Gcp proteins (Gcp7, Gcp11, and Gcp15)
515 have the same general architecture as GspC: they possess a transmembrane segment at
516 the N-terminus and a (predicted) globular domain at the C-terminus (Fig. 9A,
517 Supplementary Fig. 11). Testing possible interactions between these proteins and T2SS
518 core subunits (particularly GspG, GspF and GspDN) using BACTH or Y2H assays will
519 be of future interest.
520 Further investigations also must address the question of whether the
521 mitochondrial GspG is processed analogously to the bacterial homologues and how such
522 processing occurs in the absence of discernible homologues of GspO. The mitochondrial
523 GspG is presumably inserted into the IM by the Tim22 or Tim23 complex, resulting in a
524 GspG precursor with the N-terminus, including the MTS, protruding into the matrix. It is
525 possible that N-terminal cleavage by matrix processing peptidase serves not only to
526 remove the transit peptide, but at the same time to generate the mature N-terminus of the
527 processed GspG form, ready for recruitment into the pseudopilus. A different hypothesis
528 is offered by the discovery of the Gcp16 protein with sequence features suggesting that it
529 is a membrane-embedded metallopeptidase (certainly non-homologous to GspO, which is
530 an aspartic acid peptidase[53]). Although the subcellular localization of Gcp16 needs to be
531 established, we speculate that it might be a mitochondrial IM protein serving as an
532 alternative prepilin peptidase.
533 In parallel with its apparent simplification, the miT2SS may have been
534 specifically elaborated compared to the ancestral bacterial machinery. This possibility is
535 suggested by the existence of two pairs of proteins corresponding to different parts of the
536 bacterial GspE subunit. We propose that the eukaryotic GspE makes a heterodimer with
537 the GspEN2A to reconstitute a unit equivalent to most of the bacterial GspE protein
538 (lacking the GspL-interacting N1E domain), whereas GspEN2B, which is much more
539 divergent from the standard N2E domain than GspEN2A, may pair specifically with
540 GspEL to make an enzymatically inactive GspE-like version. We can only speculate as to
541 the function of these proteins, but the fact that the bacterial GspE assembles into a
542 homohexamer raises the possibility that in eukaryotes catalytically active and inactive
543 versions of GspE are mixed together in a manner analogous to the presence of
544 catalytically active and inactive paralogous subunits in some well-known protein
545 complexes, such as the proton-pumping ATPase (e.g. refs [54,55]). The co-occurrence of two
546 different paralogues of the GspD C-domain, one (GspDL) being particularly divergent,
547 suggests a eukaryote-specific elaboration of the putative pore in the mitochondrial OM.
548 Moreover, the electrophysiology measurements of the pores built of mitochondrial GspD
549 indicated stable complexes of variable sizes; a property not observed for bacterial
550 proteins. Finally, the C-terminal extension of the mitochondrial GspG representing a
551 novel conserved domain without discernible homology to other proteins suggests a
552 eukaryote-specific modification of the pseudopilus functioning.

553 An unanswered key question is what is the actual substrate (or substrates)
554 possibly exported from the mitochondrion by the miT2SS. No bioinformatic tool for
555 T2SS substrate prediction is available due to the enigmatic nature of the mechanism of
556 substrate recognition by the pathway[14], so at the moment we can only speculate. It is
557 notable that no protein encoded by the mitochondrial genomes of jakobids,
558 heteroloboseans and malawimonads stands out as an obvious candidate for the miT2SS
559 substrate, since they either have well-established roles in the mitochondrion or are
560 hypothetical proteins with a restricted (genus-specific) distribution. Therefore, we
561 hypothesize that the substrate could be encoded by the nuclear genome and imported into
562 the mitochondrion to undergo a specific processing/maturation step. This may include
563 addition of a prosthetic group – a scenario modelled on the process of cytochrome *c* or
564 Rieske protein maturation[56,57]. Interestingly, the proteins Gcp6 and Gcp12, each
565 exhibiting an array of absolutely conserved cysteine and histidine residues
566 (Supplementary Fig. 12), are good candidates for proteins to which a specific prosthetic
567 group might be attached, so any of them could be the sought-after miT2SS substrate.
568 Some of the other Gcp proteins may then represent components of the hypothetical
569 machinery responsible for the substrate modification. The putative functionalization step
570 may occur either in the mitochondrial matrix or in the intermembrane space (IMS), but
571 we note that the former localization would necessitate a mechanism of protein
572 translocation across the mitochondrial IM in the matrix-to-IMS direction, which has not
573 been demonstrated yet. Regardless, the T2SS system would eventually translocate the
574 modified protein across the mitochondrial OM to the cytoplasm.
575 However, this may not be the end of the journey, since there are hints of a link
576 between the miT2SS-associated pathway and peroxisomes. First, three Gcp proteins,
577 namely Gcp1 to Gcp3, are specifically related to Pex7, a protein mediating import of
578 peroxisomal proteins characterized by the peroxisomal targeting signal 2 (PTS2)[58].
579 Second, some of the Gcp proteins (especially Gcp1 and Gcp13) have at the C-terminus a
580 predicted PTS1 signal (at least in some species; Supplementary Table 1). Third, several
581 Gcp proteins (Gcp2, Gcp9, Gcp10, and Gcp11) and GspEL were assigned to the putative
582 peroxisomal proteome in our proteomic analysis (Supplementary Table 2B). We note the
583 discrepancy between the PTS1 signal predictions and the actual set of experimentally
584 defined peroxisomal proteins, which might be due to an incomplete separation of
585 peroxisome and mitochondria by our purification procedure, but may also reflect protein
586 shuttling between the two organelles. We thus hypothesize that upon its export from the
587 mitochondrion, the miT2SS substrate might be eventually delivered to the peroxisome.
588 This is possibly mediated by the Gcp1/2/3 trio, but other Gcp proteins might participate
589 as well. One such protein might be the ubiquitin-related protein Gcp4. Ubiquitination and
590 deubiquitination of several components of the peroxisome protein import machinery are a
591 critical part of the import mechanism[58] and Gcp4 might serve as an analogous peptide
592 modifier in the hypothetical novel peroxisome import pathway functionally linked to the
593 miT2SS.
594 Altogether, our data suggest the existence of a novel elaborate functional
595 pathway combining components of bacterial origin with newly evolved eukaryote-
596 specific proteins. The extant phylogenetic distribution of the pathway is sparse, but our
597 current understanding of eukaryote phylogeny suggests that it was ancestrally present in
598 eukaryotes and for some reason dispensed with multiple times during evolution.

599 Although we could not define a specific bacterial group as the actual source of the
600 eukaryotic Gsp genes, it is tempting to speculate that the T2SS was introduced into
601 eukaryotes by the bacterial progenitor of mitochondria and that it was involved in
602 delivering specific proteins from the endosymbiont into the host cell, as is known in the
603 case of current intracellular bacteria[59]. Elucidating the actual role of this communication
604 route in establishing the endosymbiont as a fully integrated organelle requires
605 understanding the cellular function of the modern miT2SS-associated pathways, which is
606 a challenge for future research.
607
608 **Methods**
609 **Sequence data and homology searches**
610 Homologues of relevant genes/proteins were searched in sequence databases accessible
611 via the National Center for Biotechnology Information BLAST server
612 (https://blast.ncbi.nlm.nih.gov/Blast.cgi), including the nucleotide and protein non-
613 redundant (nr) databases, whole-genome shotgun assemblies (WGAs), expressed
614 sequence tags (ESTs), and transcriptome shotgun assemblies (TSAs). Additional public
615 databases searched included the data provided by the Marine Microbial Eukaryote
616 Transcriptome Sequencing Project (MMETSP[60]) comprising TSAs from hundreds of
617 diverse protists (https://www.imicrobe.us/#/projects/104), the OneKP project[61]
618 (https://sites.google.com/a/ualberta.ca/onekp/) comprising TSAs from hundreds of plants
619 and algae, and individual WGAs and TSAs deposited at various on-line repositories
620 (Supplementary Table 4). To further improve the sampling, draft genome assemblies
621 were generated in this study for the heterolobosean *Neovahlkampfia damariscottae* and
622 the malawimonad informally called "*Malawimonas californiana*". Details on the
623 sequencing and assembly are provided in Supplementary Methods. Finally, the analyses
624 also included sequence data from genome and/or transcriptome projects for several
625 protists that are underway in our laboratories and will be published in full elsewhere upon
626 completion (Supplementary Table 4). Relevant sequences were extracted from these
627 unpublished datasets and either deposited in GenBank or included in Supplementary
628 Table 1.
629 Similarity searches were done using BLAST[62] (blastp or tblastn, depending on the
630 database queried) and HMMER[63] using profile HMMs built from sequence alignments of
631 proteins of interest. Hits were evaluated by BLAST (blastp or blastx) searches against the
632 nr protein dataset at NCBI to distinguish orthologues of Gsp and Gcp proteins from
633 paralogous proteins or non-specific matches. This was facilitated by a high degree of
634 conservation of individual eukaryotic Gsp/Gcp proteins among different species (see also
635 Supplementary Figs 4 and 11-13) and in most cases by the lack of other close
636 homologues in eukaryotic genomes (the exceptions being members of broader protein
637 families, including the ATPase GspE, the WD40 superfamily proteins Gcp1 to Gcp3, and
638 the ubiquitin-related protein Gcp4). All identified eukaryotic Gsp and Gcp sequences
639 were carefully manually curated to ensure maximal accuracy and completeness of the
640 data, which included correction of existing gene models, extension of truncated
641 sequences by manual analysis of raw sequencing reads, and correction of assembly errors
642 (for details see Supplementary Methods). All newly predicted or curated Gsp and Gcp
643 sequences are provided in Supplementary Table 1; additional Gsp and Gcp sequences
644 from non-target species are listed in Supplementary Table 4. The nomenclature of the

645 Gsp and Gcp genes proposed in this study was also reflected in the annotation of the *A.*
646 *godoyi* genome, recently published as part of a separate study[5].
647
648 **Phylogenetic profiling**
649 In order to identify genes with the same phylogenetic distribution as the eukaryotic
650 homologues of the four core T2SS components, we carried out two partially overlapping
651 analyses based on defining groups of putative orthologous genes in select Gsp-positive
652 species and phylogenetically diverse Gsp-negative eukaryotic species. The list of taxa
653 included is provided in Supplementary Table 5. The first analysis was based on 18
654 species, including three Gsp-positive ones (*N. gruberi*, *A. godoyi* and *M. jakobiformis*),
655 for the second analysis the set was expanded by adding one additional Gsp-positive
656 species (*G. okellyi*) and one Gsp-negative species (*Monocercomonoides exilis*). Briefly,
657 the protein sequences of a given species were compared to those of all other species using
658 blastp followed by fast phylogenetic analyses, and orthologous relationships between
659 proteins were then inferred from this set of phylogenetic trees using a reference-species-
660 tree-independent approach. This procedure was repeated for each species and all resulting
661 sets of orthologous relationships, also known as phylomes[64], were combined in a dense
662 network of orthologous relationships. This network was finally trimmed in several
663 successive steps to remove weak or spurious connections and to account for (genuine or
664 artificial) gene fusions, with the first analysis being less restrictive than the second.
665 Details of this pipeline are provided in Supplementary Methods. For each of the two
666 analyses, the final set of defined groups of orthologs (orthogroups) was parsed to identify
667 those comprising genes from at least two Gsp-positive species yet lacking genes from any
668 Gsp-negative species. The orthogroups passing this criterion were further analysed
669 manually by blastp and tblastn searches against various public and private sequence
670 repositories (see the section "Sequence data and homology searches") to exclude those
671 orthogroups with obvious orthologs in Gsp-negative species. *Percolomonas* lineage
672 exhibiting only GspD and jakobids represented by incomplete EST surveys (these species
673 likely possess the miT2SS system) were not considered Gsp-negative. The orthogroups
674 that remained were then evaluated for their conservation in Gsp-positive species and
675 those that proved to have a representative in all these species (*N. gruberi*, *N. fowleri*, *N.*
676 *damariscottae*, *P. kirbyi*, *A. godoyi*, *R. americana*, *M. jakobiformis*, *G. okellyi*) were
677 considered as bona fide Gcp (Gsp-co-occurring protein) candidates. It is of note that
678 some of these proteins are short and were missed by the automated annotation of some of
679 the genomes, so using relaxed criteria for the initial consideration of candidate
680 orthogroups (i.e. allowing for their absence from some of the Gsp-positive species)
681 proved critical for decreasing the number of false-negative identifications.
682
683 **Sequence analyses and phylogenetic inference**
684 Subcellular targeting of Gsp and Gcp proteins was evaluated using TargetP-1.1 (ref. [65];
685 http://www.cbs.dtu.dk/services/TargetP-1.1/index.php), TargetP-2.0 (ref. [66];
686 http://www.cbs.dtu.dk/services/TargetP/), Mitoprot II (ref. [67];
687 https://ihg.gsf.de/ihg/mitoprot.html), MitoFates[68] (http://mitf.cbrc.jp/MitoFates/cgi-
688 bin/top.cgi)[68], WoLF PSORT (https://wolfpsort.hgc.jp/), and PTS1 predictor[69]
689 (http://mendel.imp.ac.at/pts1/). Transmembrane domains were predicted using
690 TMHMM[70] (http://www.cbs.dtu.dk/services/TMHMM/). Homology of Gsp and Gcp

691 protein families to other proteins was evaluated by searches against Pfam v. 31 (ref. [71];
692 http://pfam.xfam.org/) and Superfamily 1.75 database[72]
693 (http://supfam.org/SUPERFAMILY/index.html), and by using HHpred[45]
694 (https://toolkit.tuebingen.mpg.de/#/tools/hhpred) and the Phyre2 server[46]
695 (http://www.sbg.bio.ic.ac.uk/phyre2/html/page.cgi?id=index). The relative position of the
696 Gcp4 family among ubiquitin-like proteins was analysed by a cluster analysis using
697 CLANS[73] (https://www.eb.tuebingen.mpg.de/protein-evolution/software/clans/); for the
698 analysis the Gcp4 family was combined with all 59 defined families included in the clan
699 Ubiquitin (CL0072) as defined in the Pfam database (each family was represented by
700 sequences from the respective seed alignments stored in the Pfam database). For further
701 details on the procedure see the legend of Supplementary Fig. 10A. Multiple sequence
702 alignments used for presentation of the conservation and specific sequence features of
703 Gsp and Gcp families were built using MUSCLE[74] and shaded using BioEdit
704 (http://www.mbio.ncsu.edu/BioEdit/bioedit.html).
705 In order to obtain datasets for the phylogenetic analyses of eukaryotic GspD to
706 GspG proteins, the protein sequences were aligned using MAFFT[75] and trimmed
707 manually. Profile hidden Markov models (HMMs) built on the basis of the respective
708 alignments were used as queries to search the UniProt database using HMMER. All
709 recovered sequences were assigned to components of the T4P superfamily machineries
710 using HMMER searches against a collection of profile HMMs reported by Abby et al.
711 (ref. [76]). For each GspD to GspG proteins, a series of alignments was built by
712 progressively expanding the sequence set by including more distant homologues (as
713 retrieved by the HMMER searches). Specifically, the different sets of sequences were
714 defined by the HMMER score based on the formula $score_{cutoff} = c*score_{best\ prokaryotic\ hit}$,
715 with the coefficient c decreasing from 0.99 to 0.70 incrementally by 0.01. The sequences
716 were then aligned using MAFFT, trimmed with BMGE[77] and the phylogenies were
717 computed with IQ-TREE[78] using the best-fit model (selected by the program from
718 standard protein evolution models and the mixture models[79] offered). The topologies
719 were tested using 10,000 ultra-fast bootstraps. The resulting trees were systematically
720 analyzed for support of the monophyly of eukaryotic sequences and for the taxonomic
721 assignment of the parental prokaryotic node of the eukaryotic subtree. The assignment
722 was done using the following procedure. The tree was artificially rooted between the
723 eukaryotic and prokaryotic sequences. From sub-leaf nodes to the deepest node of the
724 prokaryotic subtree, the taxonomic affiliation of each node was assigned by
725 proportionally considering the known or inferred taxonomic affiliations (at the phylum or
726 class level) of the descending nodes. See the legend to Supplementary Fig. 3 for further
727 details.
728 The phylogenetic analysis of the WD40 superfamily including Gcp1 to Gcp3
729 proteins was performed as follows. The starting dataset was prepared by a combination of
730 two different approaches: 1) each identified sequence of Gcp1 to Gcp3 proteins was used
731 as a query in a blastp search against the non-redundant (nr) NCBI protein database and
732 the 500 best hits for each sequence were kept; 2) protein sequences of each the Gcp1 to
733 Gcp3 family were aligned using MAFFT and the multiple alignment was used as a query
734 in a HMMER3 search (https://toolkit.tuebingen.mpg.de/#/tools/hmmer) against the
735 UniProt database. Best hits (E-value cutoff 1e-50) from the two searches were pooled and
736 de-duplicated, and the resulting sequence set (including Gcp1 to Gcp3 sequences) was

737 aligned using MAFFT and trimmed manually to remove poorly conserved regions.
738 Because WD40 proteins are extremely diversified, sequences that were too divergent
739 were eliminated from the starting dataset during three subsequent rounds of sequence
740 removal, based on a manual inspection of the alignment and phylogenetic trees computed
741 by IQ-TREE (using the best-fit model as described above). The final dataset was enriched
742 by adding PEX7 and WDR24 orthologues from eukaryotes known to possess miT2SS
743 components. The final phylogenetic tree was computed using IQ-TEE as described in the
744 legend to Supplementary Fig. 9. IQ-TREE was used also for inferring trees of the
745 heterolobosean 18S rRNA gene sequences (Supplementary Fig. 1), ubiquitin-related
746 proteins (Supplementary Fig. 10B) and the Gcp16 family (Supplementary Fig. 14);
747 details on the analyses are provided in legends to the respective figures.
748
749 **Structural homology modelling**
750 The PDB database was searched by the SWISS-MODEL server[80] for structural
751 homologues of *Go*GspD and *Go*GspG1. *V. cholerae* GspD[20] (PDB entry 5WQ9) and *K.*
752 *oxytoca* PulG[47] pseudopilus (PDB entry 5WDA) were selected as the top matches,
753 respectively. Models were built based on the target-template alignment using ProMod3
754 (ref. [80]). Coordinates that were conserved between the target and the template were
755 copied from the template to the model. Insertions and deletions were remodelled using a
756 fragment library, followed by rebuilding side chains. Finally, the geometry of the
757 resulting model was regularized by using a force field. In the case of loop modelling with
758 ProMod3 fails, an alternative model was built with PROMOD-II (ref. [81]). The quaternary
759 structure annotation of the template was used to model the target sequence in its
760 oligomeric form[82].
761
762 **Cultivation and fractionation of *N. gruberi* and proteomic analysis**
763 *Naegleria gruberi* str. NEG-M was axenically cultured in M7 medium with PenStrep
764 (100 U/mL of penicillin and 100 μg/mL of streptomycin) at 27°C in vented tissue culture
765 flasks. Mitochondria of *N. gruberi* were isolated in seven independent experiments and
766 were analyzed individually (see below). Each time ~1×10^9 *N. gruberi* cells were
767 resuspended in 2 mL of SM buffer (250 mM sucrose, 20 mM MOPS, pH 7.4)
768 supplemented with DNase I (40 μg/mL) and Roche cOmplete™ EDTA-free Protease
769 Inhibitor Cocktail and homogenized by eight passages through a 33-gauge hypodermic
770 needle (Sigma Aldrich). The resulting cell homogenate was then cleaned of cellular
771 debris using differential centrifugation and separated by a 2-hr centrifugation in a
772 discontinuous density OptiPrep gradient (10%, 15%, 20%, 30% and 50%) as described
773 previously[83]. Three visually identifiable fractions corresponding to 10-15% (OPT-1015),
774 15-20% (OPT-1520) and 20-30% (OPT-2023) OptiPrep densities were collected (each in
775 five biological replicates) and washed with SM buffer.
776 Proteins extracted from these samples were then digested with trypsin and
777 peptides were separated by nanoflow liquid chromatography and analyzed by tandem
778 mass spectrometry (nLC-MS2) on a Thermo Orbitrap Fusion (q-OT-IT) instrument as
779 described elsewhere[84]. The quantification of mass spectrometry data in the MaxQuant
780 software[85] provided normalized intensity values for 4,198 proteins in all samples and all
781 three fractions. These values were further processed using the Perseus software[86]. Data
782 were filtered and only proteins with at least two valid values in one fraction were kept.

783 Imputation of missing values, which represent low-abundance measurements, was
784 performed with random distribution around the value of instrument sensitivity using
785 default settings of Perseus software[86].
786 The data were analyzed by principle component analysis (PCA). The first two
787 loadings of the PCA were used to plot a two-dimensional graph. Based on a set of marker
788 proteins (376 mitochondrial and 26 peroxisomal, Supplementary Table 2), clusters of
789 proteins co-fractionating with mitochondria and peroxisomes were defined and the
790 proteins within the clusters were further analyzed. This workflow was set up on the basis
791 of the LOPIT protocol[87]. As a result, out of the 4,198 proteins detected, 946 putative
792 mitochondrial and 78 putative peroxisomal proteins were defined. All proteins were
793 subjected to *in silico* predictions concerning their function (BLAST, HHpred[45]) and
794 subcellular localization (Psort II, https://psort.hgc.jp/form2.html; TargetP,
795 http://www.cbs.dtu.dk/services/TargetP/; MultiLoc2, https://abi.inf.uni-
796 tuebingen.de/Services/MultiLoc2).
797
798 **Fluorescence *in situ* hybridization (FISH)**
799 The PCR products of the *NgGspE* and *NgGspF* genes were labelled by alkali-stable
800 digoxigenin-11-dUTP (Roche) using DecaLabel DNA Labeling Kit (Thermo Scientific).
801 Labelled probes were purified on columns of QIAquick Gel Extraction Kit (Qiagen,
802 28704) in a final volume of 50 µL. Labelling efficiencies were tested by dot blotting with
803 anti-digoxigenin alkaline phosphatase conjugate and CSPD chemiluminescence substrate
804 for alkaline phosphatase from DIG High Prime DNA Labelling and Detection Starter Kit
805 II (Roche) according to the manufacturer`s protocol. FISH with digoxigenin-labelled
806 probes was performed essentially according to the procedure described in Zubacova at
807 al.[88] with some modifications. *N. gruberi* cells were pelleted by centrifugation for 10 min
808 at 2,000 × g at 4°C. Cells were placed in hypotonic solution, fixed twice with a freshly
809 prepared mixture of methanol and acetic acid (3:1) and dropped on superfrost microscope
810 slides (ThermoScientific). Preparations for hybridizations were treated with RNase A, 20
811 µg in 100 µL 2 × SSC, for 1 hr at 37°C, washed twice in 2 × SSC for 5 min, dehydrated
812 in a methanol series and air-dried. Slides were treated with 50% acetic acid followed by
813 pepsin treatment and postfixation with 2% paraformaldehyde. Endogenous peroxidase
814 activity of the cell remnants (undesirable for tyramide signal amplification) was
815 inactivated by incubation in 1% hydrogen peroxide, followed by dehydration in a graded
816 methanol series. All slides were denatured together with 2 µL (25 ng) of the probe in 50
817 µL of hybridization mixture containing 50% deionised formamide (Sigma) in 2 × SSC for
818 5 min at 82°C. Hybridizations were carried out overnight. Slides were incubated with
819 tyramide reagent for 7 min. Preparations were counterstained with DAPI in VectaShield
820 and observed under an Olympus IX81 microscope equipped with a Hamamatsu Orca-AG
821 digital camera using the Cell^R imaging software.
822
823 **Heterologous gene expression, preparation of antibodies**
824 The selected Gsp genes from *G. okellyi* and *N. gruberi* were amplified from
825 commercially synthesized templates (Genscript; for primers used for PCR amplification
826 of the coding sequences see Supplementary Table 6) and cloned into the pUG35 vector.
827 The constructs were introduced into *S. cerevisiae* strain YPH499 by the lithium
828 acetate/PEG method. The positive colonies grown on SD-URA plates were incubated

829 with MitoTracker Red CMXRos (Thermo Fisher Scientific) and observed for GFP and
830 MitoTracker fluorescence (using the same equipment as used for FISH, see above). For
831 the expression in *T. brucei,* sequences encoding full-length *Go*GspD, *Go*GspG2,
832 *Ng*GspG1 as well as the first 160 amino acid residues from *Ng*GspG1 were amplified
833 from the commercially synthesized templates and cloned into the pT7 plasmid, encoding
834 either three C-terminal V5 tags (full-length genes) or C-terminal mNeonGreen followed
835 by three V5 tags (*Ng*GspG1 targeting sequence). *T. brucei* cell line SMOX 927 (ref. [89])
836 were grown in SDM79 media[90] supplemented with 10% fetal bovine serum (Gibco).
837 *NotI*-linearized plasmids (50 µg) were nucleofected into procyclic *T. brucei* cells using an
838 Amaxa nucleofector (Lonza) as described before[91]. Expression of the genes was induced
839 by an overnight incubation with doxycycline (1 µg/ml). For bacterial expression, genes
840 encoding *Ng*GspG1 and *Ng*GspEN2A were amplified from commercially synthesized
841 templates and cloned into the pET42b vector (for primers used for PCR amplification of
842 the coding sequences, see Supplementary Table 6). The constructs were introduced into
843 the chemically-competent *E. coli* strain BL21(DE3) and their expression induced by 1
844 mM IPTG. The recombinant proteins were purified under denaturing conditions on Ni-
845 NTA agarose (Qiagen). The purified proteins were used for rat immunization in an in-
846 house animal facility at the Charles University.
847
848 **Immunofluorescence microscopy**
849 Yeast, procyclic *T. brucei* or *N. gruberi* cells were pre-treated by incubation with
850 MitoTracker CMX Ros (1:000 dilution) for 20 min to stain mitochondria, washed twice
851 in PBS and placed on coverslips. After a 5-min incubation, the cells were fixed with 4%
852 PFA in PBS for 15 min. The solution was replaced by 0.1% Triton X-100 in PBS and the
853 slides were incubated for 15 min. The slides were then treated with blocking buffer (1%
854 BSA and 0.033% Triton X-100 in PBS) for 1 hr at room temperature. After blocking, the
855 samples were stained overnight at 4°C with a blocking solution supplemented with the
856 primary antibody (in-house-produced rat anti-*Ng*GspG1 and anti-*Ng*GspEN2A
857 antibodies, dilutions 1:100, rat anti-V5 antibody Abcam, dilution 1:1000 dilution). The
858 slides were washed three times for 10 min with 0.033% Triton X-100 and incubated with
859 an anti-rat antibody conjugated with Alexa Fluor® 488 (1:1000 dilution, Thermo Fisher
860 Scientific) in blocking buffer for 1 hr at room temperature. Slides were washed twice in
861 PBS supplemented with 0.033% Triton X-100 for 10 min followed by a single 10-min
862 wash with PBS only. The slides were mounted in Vectashield containing DAPI (Vector
863 laboratories). Static images were acquired on a Leica SP8 FLIM inverted confocal
864 microscope equipped with 405 nm and white light (470-670 nm) lasers and a FOV SP8
865 scanner using an HC PL APO CS2 63x/1.4 NA oil-immersion objective. Laser
866 wavelengths and intensities were controlled by a combination of AOTF and AOBS
867 separately for each channel. Emitting fluorescence was captured by internal spectrally-
868 tunable HyD detectors. Imaging was controlled by the Leica LAS-X software. Images
869 were deconvolved using the SVI Huygens Professional software (Scientific Volume
870 Imaging) with the CMLE algorithm. Maximum intensity projections and
871 brightness/contrast corrections were performed in the FIJI ImageJ software.
872
873 **Purification of native *Ng*GspD and *Ng*GspG**

874 His-tagged *Ng*GspD carrying the signal peptide of *E. coli* DsbA was produced in the *E.*
875 *coli* strain BL21 (DE3) in auto-induction media (50 mM Na_2HPO_4, 50 mM KH_2PO_4, 2%
876 Tryptone, 0.5% Yeast extract, 85 mM NaCl, 0.5% glycerol, 0.05% glucose and 0.2%
877 lactose) as described in ref. [92]. The cells were grown at 37°C for 16 hr, centrifuged at
878 6,000 × g for 15 min at 4°C and resuspended in 20 mM Tris pH 8, 5 mM EDTA. Bacteria
879 were incubated for 30 min on ice in the presence of lysozyme (1 mg/ml) and DNAse, and
880 lysed in a French press. The cell lysate was centrifuged at 6,000 × g for 15 min at 4°C to
881 pellet cell debris. The cleared lysate was then centrifuged at 100,000 × g for 2 h at 4°C
882 and membrane pellet was washed twice in 20 mM Tris pH 8, with 1-hr centrifugation
883 steps (100,000 × g at 4°C). The membranes were resuspended to the final protein
884 concentration of 1 mg/ml in 50 mM Tris pH 8, 250 mM NaCl, 1% Zwittergent 3-14, and
885 solubilized for 2 hr at 4°C. The sample was then centrifuged at 100,000 × g for 1 hr at
886 4°C. His-tagged proteins from the supernatant were incubated overnight with Ni-NTA
887 agarose (Qiagen) at 4°C. The next day, the agarose was collected on a column and
888 washed with 50 ml of 50 mM Tris pH 8, 250 mM NaCl, 20 mM Imidazole, 0.5%
889 Zwittergent 3-14. Bound proteins were eluted by 5 × 0.5 ml of 50 mM Tris pH 8, 250
890 mM NaCl, 250 mM imidazole, Zwittergent 3-14. Collected fractions were analyzed by
891 SDS PAGE and western blotting. Selected samples were then pooled together, re-
892 buffered into 50 mM Tris pH 8, 250 mM NaCl, 0.5% Zwittergent 3-14, and analyzed by
893 size exclusion chromatography.
894 For *Ng*GspG1, the BL21 cells expressing the pseudopilin domain lacking the N-
895 terminal hydrophobic part were collected after 4 hr of IPTG induction at 37°C. The cells
896 were collected, washed with PBS, and then resuspended in 35 ml of 50 mM Tris, 100
897 mM NaCl, pH 8 with added inhibitors (cOMPLETE™ tablets, EDTA-free, Roche),
898 DNAse (1 mg/ml), 5 mM $MgCl_2$ and lysozyme (1 mg/ml). The suspension was incubated
899 on ice for 30 min. After lysis via French press the resulting suspension was spun down
900 for 20 min at 100,000 × g, 4 °C. Ni-NTA agarose beads (1 ml; Qiagen), washed and
901 resuspended in loading buffer (50 mM Tris, 100 mM NaCl, 10 mM imidazole, pH 8),
902 were added to the supernatant. The supernatant was incubated with the beads for 1 hr on a
903 tube rotator at 4°C. The suspension was then applied to a column. The beads on the
904 column were then washed with 8 ml of wash buffer (50mM Tris, 100 mM NaCl, 20 mM
905 imidazole, pH 8). The protein was eluted by 4 ml elution buffer I (50 mM Tris, 100 mM
906 NaCl, 100 mM imidazole, pH 8) and 4 ml of elution buffer II (50 mM Tris, 100 mM
907 NaCl, 150 mM imidazole, pH 8). All elutions were then rebuffered to 50 mM Tris pH 8,
908 100 mM NaCl, using Amicon Ultra-4 10k centrifugal filter tubes. The protein binding
909 was measured by the microscale thermophoresis technique on a Monolith NT.115
910 instrument (Nanotemper). Protein (10 nM) in 50 mM HEPES buffer with 50 mM NaCl
911 was labelled with Red-NHS dye NT-647. Maximum concentration of titrated protein was
912 50 µM.
913
914 **Black lipid membrane measurements**
915 Planar lipid membrane experiments were performed as described previously[93]. The
916 electrolyte solution contained 1 M KCl and 10 mM Tris-HCl (pH 7.4). 5 µl of purified
917 protein (80 ng/ml) was mixed with 1500 µl KCl and was added to the *cis* compartment
918 with a positive electrode, whereas the *trans* compartment was grounded. Planar lipid
919 membrane was formed across a 0.5-mm aperture by painting the *E. coli* polar lipids

920 extract (3% wt/vol, Avanti Polar Lipids, Alabaster, USA) dissolved in *n*-decan and
921 butanol (9:1). The membrane current was registered using Ag/AgCl electrodes with salt
922 bridges connected to an LCA-200-10G amplifier (Femto, Germany) and digitized with a
923 KPCI-3108 16-Bit A/D card (Keithley Instruments, USA) with a 1-kHz sampling rate.
924 Single-pore recordings were processed in the program QuB[94]. The histogram of single-
925 pore conductance (n=100) was constructed by kernel density estimation (with the
926 Gaussian kernel of 100-pS width) to overcome bin edge effects.
927
928 ***In vitro* protein translation and mitochondrial protein import**
929 The *Go*GspD and *Ng*GspD genes were amplified from commercially synthesized
930 templates (for primers used for PCR amplification of the coding sequences, see
931 Supplementary Table 6) and cloned into pDHFR vector provided in the PURExpress *In*
932 *Vitro* Protein Synthesis Kit (NEB). The translation into liposomes was done as described
933 previously[95] and the output was analyzed by Blue Native PAGE using 2% digitonin and
934 NativePAGE Novex 4-16% Bis-Tris Protein Gel (Thermo Fisher Scientific). For the *in*
935 *vitro* mitochondrial protein import, the mitochondria were isolated from *S. cerevisiae*
936 YPH499 according to the method described in ref. [96]. The *in vitro*-translated *Ng*GspD and
937 Su9-DHFR chimeric construct[41] were incubated with mitochondria as described in ref. [97].
938 The import reactions were incubated with 50 µg/ml of trypsin for 30 min on ice to
939 remove unimported protein precursor.
940
941 **Testing protein interactions using two-hybrid systems**
942 Bacterial two-hybrid system (BACTH) analysis was performed as described before[98].
943 Gsp genes were amplified with specific primers (listed in Supplementary Table 6) and
944 cloned into pKT25 and pUT18c plasmids. *E. coli* strain DHT1 competent cells were co-
945 transformed with two plasmids with different combinations of Gsp genes. Co-
946 transformants were selected on LB plates with ampicillin (Ap) (100 µg/mL) and
947 kanamycin (Km) (25 µg/mL). Colonies were grown at 30°C for 48 to 96 hr. From each
948 plate three colonies were picked, transferred to 1 mL of LB medium with Ap and Km,
949 and grown overnight at 30°C with shaking. Next day, precultures (0.25 mL) were
950 inoculated to 5 mL of LB medium with Ap, Km and 1 mM IPTG. Cultures were grown
951 with shaking at 30°C to OD_{600} of about 1-1.5. Bacteria (0.5 mL) were mixed with 0.5 mL
952 of Z buffer and β-galactosidase activity was measured[99].
953 The yeast two-hybrid system (Y2H) was employed as described in ref. [100]. Cells
954 of *S. cerevisiae* strain AH109 were co-transformed with two plasmids (pGADT7,
955 pGBKT7) with different combinations of Gsp genes. Co-transformants were selected on
956 double-dropout SD-Leu/-Trp and triple-dropout SD-Leu/-Trp/-His plates. The colonies
957 were grown for a few days. Positive colonies from the triple dropout were grown
958 overnight at 30°C with shaking and then the serial dilution test was performed on double-
959 and triple-dropout plates.
960
961 **Data availability**
962 All sequences of Gsp and Gcp proteins analysed in the study are provided in
963 Supplementary Table 1. Gsp and Gcp genes extracted from an unpublished *Malawimonas*
964 *jakobiformis* genome assembly have been deposited at GenBank with accession numbers
965 MT460910-MT460938. Raw genome sequencing reads from "*Malawimonas*

966 *californiana*" and *Neovahlkampfia damariscottae* are available from NCBI under the
967 BioProject PRJNA549687. The genome assembly of *N. damariscottae* has been
968 deposited at GenBank with the accession number JABLTG000000000. The transcriptome
969 assembly of *Gefionella okellyi*, the genome assembly and predicted proteins of
970 "*Malawimonas californiana*", and partial genome assemblies of *Reclinomonas americana*
971 are available from https://megasun.bch.umontreal.ca/papers/T2SS-2020/. The mass
972 spectrometry proteomics data have been deposited in the ProteomeXchange Consortium
973 via the PRIDE[101] partner repository with the dataset identifier PXD007764. Other
974 relevant data (e.g. multiple sequence alignments used for phylogenetic analyses) are
975 available from the authors upon request.
976
977 **References**
978

979 1. Roger, A. J., Muñoz-Gómez, S. A. & Kamikawa, R. The origin and diversification
980 of mitochondria. *Curr. Biol.* **27**, R1177–R1192 (2017).
981 2. Martijn, J., Vosseberg, J., Guy, L., Offre, P. & Ettema, T. J. G. Deep mitochondrial
982 origin outside the sampled alphaproteobacteria. *Nature* **557**, 101–105 (2018).
983 3. Leger, M. M. *et al.* An ancestral bacterial division system is widespread in
984 eukaryotic mitochondria. *Proc. Natl. Acad. Sci. U. S. A.* **112**, 10239–46 (2015).
985 4. Beech, P. L. Mitochondrial FtsZ in a chromophyte alga. *Science* **287**, 1276–1279
986 (2000).
987 5. Gray, M. W. *et al.* The draft nuclear genome sequence and predicted mitochondrial
988 proteome of Andalucia godoyi, a protist with the most gene-rich and bacteria-like
989 mitochondrial genome. *BMC Biol.* **18**, (2020).
990 6. Natale, P., Brüser, T. & Driessen, A. J. M. Sec- and Tat-mediated protein secretion
991 across the bacterial cytoplasmic membrane—Distinct translocases and
992 mechanisms. *Biochim. Biophys. Acta - Biomembr.* **1778**, 1735–1756 (2008).
993 7. Costa, T. R. D. *et al.* Secretion systems in Gram-negative bacteria: structural and
994 mechanistic insights. *Nat. Rev. Microbiol.* **13**, 343–359 (2015).
995 8. Dolezal, P., Likic, V., Tachezy, J. & Lithgow, T. Evolution of the molecular
996 machines for protein import into mitochondria. *Science* **313**, 314–8 (2006).
997 9. Petru, M. *et al.* Evolution of mitochondrial TAT translocases illustrates the loss of
998 bacterial protein transport machines in mitochondria. *BMC Biol.* **16**, (2018).
999 10. Schäfer, K., Künzler, P., Klingl, A., Eubel, H. & Carrie, C. The plant
1000 mitochondrial TAT pathway is essential for complex III biogenesis. *Curr. Biol.* **30**,
1001 840-853.e5 (2020).
1002 11. Lang, B. F. *et al.* An ancestral mitochondrial DNA resembling a eubacterial
1003 genome in miniature. *Nature* **387**, 493–7 (1997).
1004 12. Burger, G., Gray, M. W., Forget, L. & Lang, B. F. Strikingly bacteria-like and
1005 gene-rich mitochondrial genomes throughout jakobid protists. *Genome Biol. Evol.*
1006 **5**, 418–38 (2013).
1007 13. Tong, J. *et al.* Ancestral and derived protein import pathways in the mitochondrion
1008 of *Reclinomonas america*. *Mol. Biol. Evol.* **28**, 1581–91 (2011).
1009 14. Korotkov, K. V., Sandkvist, M. & Hol, W. G. J. The type II secretion system:
1010 biogenesis, molecular architecture and mechanism. *Nat. Rev. Microbiol.* **10**, 336–
1011 51 (2012).

1012 15. Thomassin, J.-L., Santos Moreno, J., Guilvout, I., Tran Van Nhieu, G. & Francetic,
1013 O. The trans-envelope architecture and function of the type 2 secretion system:
1014 new insights raising new questions. *Mol. Microbiol.* **105**, 211–226 (2017).
1015 16. Berry, J.-L. & Pelicic, V. Exceptionally widespread nanomachines composed of
1016 type IV pilins: the prokaryotic Swiss Army knives. *FEMS Microbiol. Rev.* **39**,
1017 134–54 (2015).
1018 17. Nivaskumar, M. & Francetic, O. Type II secretion system: a magic beanstalk or a
1019 protein escalator. *Biochim. Biophys. Acta* **1843**, 1568–77 (2014).
1020 18. Denise, R., Abby, S. S. & Rocha, E. P. C. Diversification of the type IV filament
1021 superfamily into machines for adhesion, protein secretion, DNA uptake, and
1022 motility. *PLoS Biol.* **17**, e3000390 (2019).
1023 19. Guilvout, I. *et al.* In vitro multimerization and membrane insertion of bacterial
1024 outer membrane secretin PulD. *J. Mol. Biol.* **382**, 13–23 (2008).
1025 20. Yan, Z., Yin, M., Xu, D., Zhu, Y. & Li, X. Structural insights into the secretin
1026 translocation channel in the type II secretion system. *Nat. Struct. Mol. Biol.* **24**,
1027 177–183 (2017).
1028 21. Py, B., Loiseau, L. & Barras, F. An inner membrane platform in the type II
1029 secretion machinery of Gram-negative bacteria. *EMBO Rep.* **2**, 244–248 (2001).
1030 22. Wang, X. *et al.* Cysteine scanning mutagenesis and disulfide mapping analysis of
1031 arrangement of GspC and GspD protomers within the type 2 secretion system. *J.*
1032 *Biol. Chem.* **287**, 19082–93 (2012).
1033 23. Korotkov, K. V. *et al.* Structural and functional studies on the interaction of GspC
1034 and GspD in the type II secretion system. *PLoS Pathog.* **7**, e1002228 (2011).
1035 24. Korotkov, K. V & Hol, W. G. J. Structure of the GspK-GspI-GspJ complex from
1036 the enterotoxigenic Escherichia coli type 2 secretion system. *Nat. Struct. Mol. Biol.*
1037 **15**, 462–8 (2008).
1038 25. Peabody, C. R. *et al.* Type II protein secretion and its relationship to bacterial type
1039 IV pili and archaeal flagella. *Microbiology* **149**, 3051–72 (2003).
1040 26. Lu, C. *et al.* Hexamers of the type II secretion ATPase GspE from Vibrio cholerae
1041 with Increased ATPase activity. *Structure* **21**, 1707–1717 (2013).
1042 27. Lax, G. *et al.* Hemimastigophora is a novel supra-kingdom-level lineage of
1043 eukaryotes. *Nature* **564**, 410–414 (2018).
1044 28. Adl, S. M. *et al.* The revised classification of eukaryotes. *J. Eukaryot. Microbiol.*
1045 **59**, 429–514 (2012).
1046 29. Derelle, R. *et al.* Bacterial proteins pinpoint a single eukaryotic root. *Proc. Natl.*
1047 *Acad. Sci. U. S. A.* **112**, E693-9 (2015).
1048 30. Karnkowska, A. *et al.* A eukaryote without a mitochondrial organelle. *Curr. Biol.*
1049 **26**, 1274–84 (2016).
1050 31. Heiss, A. A. *et al.* Combined morphological and phylogenomic re-examination of
1051 malawimonads, a critical taxon for inferring the evolutionary history of
1052 eukaryotes. *R. Soc. Open Sci.* **5**, 171707 (2018).
1053 32. Brown, M. W. *et al.* Phylogenomics places orphan protistan lineages in a novel
1054 eukaryotic super-group. *Genome Biol. Evol.* **10**, 427–433 (2018).
1055 33. Mach, J. *et al.* Iron economy in *Naegleria gruberi* reflects its metabolic flexibility.
1056 *Int. J. Parasitol.* **48**, 719–727 (2018).
1057 34. Nouwen, N. *et al.* Secretin PulD: Association with pilot PulS, structure, and ion-

1058 conducting channel formation. *Proc. Natl. Acad. Sci.* **96**, 8173–8177 (1999).
1059 35. Hardie, K. R., Lory, S. & Pugsley, A. P. Insertion of an outer membrane protein in
1060 *Escherichia coli* requires a chaperone-like protein. *EMBO J.* **15**, 978–88 (1996).
1061 36. Dunstan, R. A. *et al.* Assembly of the secretion pores GspD, Wza and CsgG into
1062 bacterial outer membranes does not require the Omp85 proteins BamA or TamA.
1063 *Mol. Microbiol.* **97**, 616–629 (2015).
1064 37. Collin, S., Guilvout, I., Chami, M. & Pugsley, A. P. YaeT-independent
1065 multimerization and outer membrane association of secretin PulD. *Mol. Microbiol.*
1066 **64**, 1350–1357 (2007).
1067 38. Korotkov, K. V, Pardon, E., Steyaert, J. & Hol, W. G. J. Crystal structure of the N-
1068 terminal domain of the secretin GspD from ETEC determined with the assistance
1069 of a nanobody. *Structure* **17**, 255–265 (2009).
1070 39. Guilvout, I. *et al.* Prepore stability controls productive folding of the BAM
1071 independent multimeric outer membrane secretin PulD. *J. Biol. Chem.* **292**, 328–
1072 338 (2017).
1073 40. Chernyatina, A. A. & Low, H. H. Core architecture of a bacterial type II secretion
1074 system. *Nat. Commun.* **10**, 5437 (2019).
1075 41. Pfanner, N., Tropschug, M. & Neupert, W. Mitochondrial protein import:
1076 Nucleoside triphosphates are involved in conferring import-competence to
1077 precursors. *Cell* **49**, 815–823 (1987).
1078 42. Yin, M., Yan, Z. & Li, X. Structural insight into the assembly of the Type II
1079 secretion system pilotin-Secretin complex from enterotoxigenic *Escherichia coli*.
1080 *Nat Microbiol* (2018). doi:10.2210/PDB5ZDH/PDB
1081 43. Guilvout, I. *et al.* In Vitro Multimerization and Membrane Insertion of Bacterial
1082 Outer Membrane Secretin PulD. *J. Mol. Biol.* **382**, 13–23 (2008).
1083 44. Sauvonnet, N., Vignon, G., Pugsley, A. P. & Gounon, P. Pilus formation and
1084 protein secretion by the same machinery in Escherichia coli. *EMBO J.* **19**, 2221–
1085 2228 (2000).
1086 45. Alva, V., Nam, S.-Z., Söding, J. & Lupas, A. N. The MPI bioinformatics Toolkit
1087 as an integrative platform for advanced protein sequence and structure analysis.
1088 *Nucleic Acids Res.* **44**, W410–W415 (2016).
1089 46. Kelley, L. A., Mezulis, S., Yates, C. M., Wass, M. N. & Sternberg, M. J. E. The
1090 Phyre2 web portal for protein modeling, prediction and analysis. *Nat. Protoc.* **10**,
1091 845–858 (2015).
1092 47. López-Castilla, A. *et al.* Structure of the calcium-dependent type 2 secretion
1093 pseudopilus. *Nat. Microbiol.* **2**, 1686–1695 (2017).
1094 48. Nivaskumar, M. *et al.* Pseudopilin residue E5 is essential for recruitment by the
1095 type 2 secretion system assembly platform. *Mol. Microbiol.* **101**, 924–41 (2016).
1096 49. Lu, C., Korotkov, K. V. & Hol, W. G. J. Crystal structure of the full-length
1097 ATPase GspE from the Vibrio vulnificus type II secretion system in complex with
1098 the cytoplasmic domain of GspL. *J. Struct. Biol.* **187**, 223–235 (2014).
1099 50. Cerdà-Costa, N. & Xavier Gomis-Rüth, F. Architecture and function of
1100 metallopeptidase catalytic domains. *Protein Sci.* **23**, 123–144 (2014).
1101 51. Tabach, Y. *et al.* Identification of small RNA pathway genes using patterns of
1102 phylogenetic conservation and divergence. *Nature* **493**, 694–698 (2012).
1103 52. Nevers, Y. *et al.* Insights into ciliary genes and evolution from multi-level

1104 phylogenetic profiling. *Mol. Biol. Evol.* **34**, 2016–2034 (2017).
1105 53. McLaughlin, L. S., Haft, R. J. F. & Forest, K. T. Structural insights into the Type
1106 II secretion nanomachine. *Current Opinion in Structural Biology* **22**, 208–216
1107 (2012).
1108 54. Okuno, D., Iino, R. & Noji, H. Rotation and structure of FoF1-ATP synthase. *J.*
1109 *Biochem.* **149**, 655–664 (2011).
1110 55. Tomko, R. J. & Hochstrasser, M. Molecular architecture and assembly of the
1111 eukaryotic proteasome. *Annu. Rev. Biochem.* **82**, 415–445 (2013).
1112 56. Babbitt, S. E., Sutherland, M. C., San Francisco, B., Mendez, D. L. & Kranz, R. G.
1113 Mitochondrial cytochrome c biogenesis: no longer an enigma. *Trends Biochem.*
1114 *Sci.* **40**, 446–55 (2015).
1115 57. Hartl, F. U., Schmidt, B., Wachter, E., Weiss, H. & Neupert, W. Transport into
1116 mitochondria and intramitochondrial sorting of the Fe/S protein of ubiquinol-
1117 cytochrome c reductase. *Cell* **47**, 939–51 (1986).
1118 58. Francisco, T. *et al.* Protein transport into peroxisomes: Knowns and unknowns.
1119 *BioEssays* **39**, 1700047 (2017).
1120 59. Nguyen, B. D. & Valdivia, R. H. Virulence determinants in the obligate
1121 intracellular pathogen *Chlamydia trachomatis* revealed by forward genetic
1122 approaches. *Proc. Natl. Acad. Sci.* **109**, 1263–1268 (2012).
1123 60. Keeling, P. J. *et al.* The marine microbial eukaryote transcriptome sequencing
1124 project (MMETSP): illuminating the functional diversity of eukaryotic life in the
1125 oceans through transcriptome sequencing. *PLoS Biol.* **12**, e1001889 (2014).
1126 61. Matasci, N. *et al.* Data access for the 1,000 Plants (1KP) project. *Gigascience* **3**, 17
1127 (2014).
1128 62. Altschul, S. F. *et al.* Gapped BLAST and PSI-BLAST: a new generation of protein
1129 database search programs. *Nucleic Acids Res.* **25**, 3389–402 (1997).
1130 63. Finn, R. D., Clements, J. & Eddy, S. R. HMMER web server: interactive sequence
1131 similarity searching. *Nucleic Acids Res.* **39**, W29-37 (2011).
1132 64. Huerta-Cepas, J., Dopazo, H., Dopazo, J. & Gabaldón, T. The human phylome.
1133 *Genome Biol.* **8**, R109 (2007).
1134 65. Emanuelsson, O., Nielsen, H., Brunak, S. & von Heijne, G. Predicting subcellular
1135 localization of proteins based on their N-terminal amino acid sequence. *J. Mol.*
1136 *Biol.* **300**, 1005–16 (2000).
1137 66. Armenteros, J. J. A. *et al.* Detecting sequence signals in targeting peptides using
1138 deep learning. *Life Sci. Alliance* **2**, (2019).
1139 67. Claros, M. G. MitoProt, a Macintosh application for studying mitochondrial
1140 proteins. *Comput. Appl. Biosci.* **11**, 441–7 (1995).
1141 68. Fukasawa, Y. *et al.* MitoFates: improved prediction of mitochondrial targeting
1142 sequences and their cleavage sites. *Mol. Cell. Proteomics* **14**, 1113–26 (2015).
1143 69. Neuberger, G., Maurer-Stroh, S., Eisenhaber, B., Hartig, A. & Eisenhaber, F.
1144 Prediction of peroxisomal targeting signal 1 containing proteins from amino acid
1145 sequence. *J. Mol. Biol.* **328**, 581–92 (2003).
1146 70. Käll, L., Krogh, A. & Sonnhammer, E. L. L. Advantages of combined
1147 transmembrane topology and signal peptide prediction--the Phobius web server.
1148 *Nucleic Acids Res.* **35**, W429-32 (2007).
1149 71. Finn, R. D. *et al.* The Pfam protein families database: towards a more sustainable

1150 future. *Nucleic Acids Res.* **44**, D279-85 (2016).
1151 72. de Lima Morais, D. A. *et al.* SUPERFAMILY 1.75 including a domain-centric
1152 gene ontology method. *Nucleic Acids Res.* **39**, D427-34 (2011).
1153 73. Frickey, T. & Lupas, A. CLANS: a Java application for visualizing protein
1154 families based on pairwise similarity. *Bioinformatics* **20**, 3702–3704 (2004).
1155 74. Edgar, R. C. MUSCLE: multiple sequence alignment with high accuracy and high
1156 throughput. *Nucleic Acids Res.* **32**, 1792–7 (2004).
1157 75. Katoh, K. & Standley, D. M. MAFFT multiple sequence alignment software
1158 version 7: improvements in performance and usability. *Mol. Biol. Evol.* **30**, 772–
1159 780 (2013).
1160 76. Abby, S. S. *et al.* Identification of protein secretion systems in bacterial genomes.
1161 *Sci. Rep.* **6**, 23080 (2016).
1162 77. Criscuolo, A. & Gribaldo, S. BMGE (Block Mapping and Gathering with
1163 Entropy): a new software for selection of phylogenetic informative regions from
1164 multiple sequence alignments. *BMC Evol. Biol.* **10**, 210 (2010).
1165 78. Nguyen, L.-T., Schmidt, H. A., von Haeseler, A. & Minh, B. Q. IQ-TREE: a fast
1166 and effective stochastic algorithm for estimating maximum-likelihood
1167 phylogenies. *Mol. Biol. Evol.* **32**, 268–74 (2015).
1168 79. Lartillot, N. & Philippe, H. A Bayesian mixture model for across-site
1169 heterogeneities in the amino-acid replacement process. *Mol. Biol. Evol.* **21**, 1095–
1170 109 (2004).
1171 80. Bienert, S. *et al.* The SWISS-MODEL Repository-new features and functionality.
1172 *Nucleic Acids Res.* **45**, D313–D319 (2017).
1173 81. Guex, N., Peitsch, M. C. & Schwede, T. Automated comparative protein structure
1174 modeling with SWISS-MODEL and Swiss-PdbViewer: A historical perspective.
1175 *Electrophoresis* **30**, S162–S173 (2009).
1176 82. Biasini, M. *et al.* SWISS-MODEL: modelling protein tertiary and quaternary
1177 structure using evolutionary information. *Nucleic Acids Res.* **42**, W252-8 (2014).
1178 83. Jedelský, P. L. *et al.* The minimal proteome in the reduced mitochondrion of the
1179 parasitic protist *Giardia intestinalis*. *PLoS One* **6**, e17285 (2011).
1180 84. Černá, M., Kuntová, B., Talacko, P., Stopková, R. & Stopka, P. Differential
1181 regulation of vaginal lipocalins (OBP, MUP) during the estrous cycle of the house
1182 mouse. *Sci. Rep.* **7**, 11674 (2017).
1183 85. Cox, J. *et al.* Accurate proteome-wide label-free quantification by delayed
1184 normalization and maximal peptide ratio extraction, termed MaxLFQ. *Mol. Cell.*
1185 *Proteomics* **13**, 2513–2526 (2014).
1186 86. Tyanova, S. *et al.* The Perseus computational platform for comprehensive analysis
1187 of (prote)omics data. *Nat. Methods* **13**, 731–740 (2016).
1188 87. Dunkley, T. P. J., Watson, R., Griffin, J. L., Dupree, P. & Lilley, K. S.
1189 Localization of organelle proteins by isotope tagging (LOPIT). *Mol. Cell.*
1190 *Proteomics* **3**, 1128–1134 (2004).
1191 88. Zubáčová, Z., Krylov, V. & Tachezy, J. Fluorescence in situ hybridization (FISH)
1192 mapping of single copy genes on *Trichomonas vaginalis* chromosomes. *Mol.*
1193 *Biochem. Parasitol.* **176**, 135–137 (2011).
1194 89. Poon, S. K., Peacock, L., Gibson, W., Gull, K. & Kelly, S. A modular and
1195 optimized single marker system for generating *Trypanosoma brucei* cell lines

expressing T7 RNA polymerase and the tetracycline repressor. *Open Biol.* **2**, 110037 (2012).
90. Brun, R. & Schönenberger. Cultivation and *in vitro* cloning or procyclic culture forms of Trypanosoma brucei in a semi-defined medium. Short communication. *Acta Trop.* **36**, 289–92 (1979).
91. Kaurov, I. *et al.* The diverged trypanosome MICOS complex as a hub for mitochondrial cristae shaping and protein import. *Curr. Biol.* **28**, 3393-3407.e5 (2018).
92. Studier, F. W. Protein production by auto-induction in high-density shaking cultures. (2005). doi:10.1016/j.pep.2005.01.016
93. Seydlová, G. *et al.* Lipophosphonoxins II: design, synthesis, and properties of novel broad spectrum antibacterial agents. *J. Med. Chem.* **60**, 6098–6118 (2017).
94. Nicolai, C. & Sachs, F. Solving ion channel kinetics with the QuB software. *Biophys. Rev. Lett.* **08**, 191–211 (2013).
95. Pyrihová, E. *et al.* A Single Tim translocase in the mitosomes of *Giardia intestinalis* illustrates convergence of protein import machines in anaerobic eukaryotes. *Genome Biol. Evol.* **10**, 2813–2822 (2018).
96. Daum, G., Böhni, P. C. & Schatz, G. Import of proteins into mitochondria. Cytochrome b2 and cytochrome c peroxidase are located in the intermembrane space of yeast mitochondria. *J. Biol. Chem.* **257**, 13028–13033 (1982).
97. Dolezal, P. *et al.* Legionella pneumophila secretes a mitochondrial carrier protein during infection. *PLoS Pathog.* **8**, e1002459 (2012).
98. Battesti, A. & Bouveret, E. The bacterial two-hybrid system based on adenylate cyclase reconstitution in *Escherichia coli*. *Methods* **58**, 325–334 (2012).
99. Miller, J. H. *Experiments in molecular genetics*. (Cold Spring Harbor Laboratory, 1972).
100. Fields, S. & Song, O. A novel genetic system to detect protein-protein interactions. *Nature* **340**, 245–246 (1989).
101. Vizcaíno, J. A. *et al.* 2016 update of the PRIDE database and its related tools. *Nucleic Acids Res.* **44**, 11033–11033 (2016).
102. Adl, S. M. *et al.* Revisions to the classification, nomenclature, and diversity of eukaryotes. *J. Eukaryot. Microbiol.* **66**, 4–119 (2019).
103. Strassert, J. F. H., Jamy, M., Mylnikov, A. P., Tikhonenkov, D. V & Burki, F. New Phylogenomic Analysis of the Enigmatic Phylum Telonemia Further Resolves the Eukaryote Tree of Life. *Mol. Biol. Evol.* **36**, 757–765 (2019).

Acknowledgements

We would like to thank Michelle Leger and Alastair Simpson for granting us access, prior to publication, to their transcriptomic data from *A. godoyi* and *G. okellyi*, respectively, data that were instrumental in annotating the Gsp and Gcp genes in our genome assemblies. This work was supported by Czech Science Foundation grants 13-29423S to PD and 18-18699S to ME, and the KONTAKT II grant LH15253 provided by Ministry of Education, Youth and Sports of CR (MEYS) to PD. This work was also supported by MEYS within the National Sustainability Program II (Project BIOCEV-FAR, LQ1604) the project BIOCEV (CZ.1.05/1.1.00/02.0109), and the project "Centre for research of

pathogenicity and virulence of parasites" (No. CZ.02.1.01/0.0/0.0/16_019/0000759) funded by European Regional Development Fund (ERDF) and MEYS and by Moore-Simons Project on the Origin of the Eukaryotic Cell to PD. The work in the OF laboratory was funded by the ANR-14-CE09-0004 grant. JP was supported by a grant from the Gordon and Betty Moore Foundation to ADT. This work was supported by The Ministry of Education, Youth and Sports from the Large Infrastructures for Research, Experimental Development and Innovations project "IT4Innovations National Supercomputing Center – LM2015070".

Author information

Affiliations

Department of Parasitology, Faculty of Science, Charles University, BIOCEV, Průmyslová 595, Vestec, 252 42, Czech Republic
L. Horváthová, V. Žárský, A. Motyčková, V. Klápšťová, M. Vinopalová, L. Marková, L. Voleman, M. Petrů, Z. Vaitová & P. Doležal

Department of Biology and Ecology, Faculty of Science, University of Ostrava, Chittussiho 10, 710 00 Ostrava, Czech Republic
T. Pánek, V. Klimeš & M. Eliáš

School of Biosciences, University of Birmingham, Edgbaston, B15 2TT, UK
R. Derelle

Laboratory of Molecular & Evolutionary Parasitology, RAPID group, School of Biosciences, University of Kent, Canterbury, CT2 7NZ, UK
J. Pyrih & A. D. Tsaousis

Department of Zoology, Faculty of Science, Charles University, Viničná 7, Prague 2, 128 44, Czech Republic
I. Čepička

Department of Genetics and Microbiology, Faculty of Science, Charles University, Viničná 7, Prague 2, 128 44, Czech Republic
K. Hryzáková

Proteomic core facility, Faculty of Science, Charles University, BIOCEV, Průmyslová 595, Vestec, 252 42, Czech Republic
K. Harant

Department of Biochemistry and Molecular Biology and Centre for Comparative Genomics and Evolutionary Bioinformatics, Dalhousie University, Halifax, NS B3H 4R2, Canada
M. W. Gray

Center for Cellular Imaging and NanoAnalytics, University of Basel, Mattenstrasse 26, CH-4058 Basel, Switzerland
M. Chami

Institut Pasteur, Biochemistry of Macromolecular Interactions Unit, Department of Structural Biology and Chemistry, CNRS UMR3528, 75015 Paris, France
I. Guilvout & O. Francetic

Robert Cedergren Centre for Bioinformatics and Genomics, Département de Biochimie, Université de Montréal, Montreal, QC, Canada H3T 1J4
B. F. Lang

Institute of Molecular Genetics, Czech Academy of Sciences, 142 20 Prague 4, Czech Republic
Č. Vlček

Author contributions

L.H. planned and carried out the experiments, V.Ž. conceived the original idea and carried out the bioinformatics analyses, T.P. obtained the *N. damariscottae* genome sequence and carried out the genome and bioinformatic analyses, R.D. designed and carried out comparative genomic analyses, J.P. planned and carried out the experiments on *N. gruberi* mitochondrial proteome and analysed the data, A.M. carried out the experiments, Ve.K. carried out the experiments, M.V. carried out the experiments, L.M. carried out the experiments, L.V. carried out the experiments Vl.K. participated in genome sequencing and analysis, M.P. planned carried out the experiments, I.Č. participated in genome data acquisition, K.H. carried out the experiments, Z.V. carried out the experiments, K.H. analysed the proteome of *N. gruberi* mitochondria, M.W.G. contributed to the interpretation of the results and manuscript preparation, M.CH. carried out the experiments and analyzed the data, I.G. designed and planned the experiments, O.F. designed, planned and carried out the experiments and analyzed the data, B.F.L. provided the genome data and analyses and contributed to manuscript preparation, Č.V. participated in genome data acquisition, A.D.T. designed and planned the experiments, M.E. conceived the idea, performed genomic analyses and wrote the manuscript, P.D. conceived the idea, designed and performed experiments and wrote the manuscript.

Competing interests

None declared.

Corresponding author

Correspondence to M. Eliáš or P. Doležal.

Figure Legends

1333 **Fig. 1 Some eukaryotes harbour homologues of core components of the bacterial**
1334 **T2SS machinery.** (A) Schematic representation of the complete bacterial T2SS; subunits
1335 having identified eukaryotic homologues are highlighted in colour. For simplicity,
1336 GspDN represents in the figure three different eukaryotic proteins (GspDN1 to GspDN3),
1337 together corresponding to two versions of a conserved domain present as a triplicate in
1338 the N-terminal region of the bacterial GspD protein. (B) Phylogenetic distribution of
1339 eukaryotic homologues of bacterial T2SS subunits (Gsp proteins) and co-occurring
1340 proteins (Gcp). Core T2SS components (cyan), eukaryote-specific T2SS components
1341 (dark blue), Gcp proteins carrying protein domains found in eukaryotes (magenta), and
1342 Gcp proteins without discernible homologues or with homologues only in prokaryotes
1343 (pink). Coloured sections indicate proteins found to be present in genome or
1344 transcriptome data; white sections, proteins absent from complete genome data; grey
1345 sections, proteins absent from transcriptome data. The asterisk indicates the presence of
1346 the particular protein in at least two of the three *Percolomonas* or at least one of the two
1347 Hemimastigophora species analyzed. The species name in parentheses has not yet been
1348 formally published. Sequence IDs and additional details on the eukaryotic Gsp and Gcp
1349 proteins are provided in Supplementary Table 1. The tree topology and taxon names
1350 reflect most recent phylogenomic studies of eukaryotes[32,102,103]; the root (LECA) is placed
1351 according to ref. [29].
1352
1353 **Fig. 2 Eukaryotic Gsp homologues are monophyletic.** Maximum likelihood (ML)
1354 phylogenetic tree of eukaryotic and selected bacterial GspG proteins demonstrating the
1355 monophyletic origin of the eukaryotic GspG proteins and their separation from bacterial
1356 homologues by a long branch (the tree inferred using IQ-TREE). Branch support
1357 (bootstrap) was assessed by ML ultrafast bootstrapping and is shown only for branches
1358 where support is > 50.
1359
1360 **Fig. 3 Eukaryotic T2SS components are localized in mitochondria.** (A) *S. cerevisiae*
1361 expressing *G. okellyi* and *N. gruberi* Gsp proteins as C-terminal GFP fusions stained with
1362 MitoTracker red CMX ROS to visualize mitochondria. (B) Expression of *G. okellyi*
1363 GspD and GspG2 with the C-terminal V5 Tag in *T. brucei* visualized by
1364 immunofluorescence; the cells are co-stained with MitoTracker red. (C) Cellular fractions
1365 of *N. gruberi* labelled by specific polyclonal antibodies raised against GspG1, GspEN2A
1366 and mitochondrial (alternative oxidase – AOX, TatC,) cytosolic (hemerythrin) marker
1367 proteins. (D) Immunofluorescence microscopy of *N. gruberi* labelled with specific
1368 polyclonal antibodies raised against GspG1 and GspEN2A, and co-stained with
1369 MitoTracker red. Scale bar (parts A-D), 10 µm. (E) PCA analysis of 4,198 proteins
1370 identified in the proteomic analysis of *N. gruberi* subcellular fractions differentially
1371 enriched in mitochondria. The cluster of mitochondrial proteins was defined on the basis
1372 of 376 mitochondrial markers. The boundaries of the cluster of co-purified peroxisomal
1373 proteins were defined by 26 peroxisomal markers.
1374
1375 **Fig. 4 Mitochondrial GspD oligomerizes towards the formation of membrane pores.**
1376 (A) Domain architecture of the canonical bacterial GspD and the eukaryotic proteins
1377 homologous to its different parts (short N-terminal region of mitochondrial GspD of
1378 unidentified homology shown in grey). Below, protein sequence alignment of the secretin

1379 C-domain of bacterial and mitochondrial orthologues (mitochondrial GspD or GspDL
1380 and the respective molecular complex of bacterial secretins is depicted in grey, the
1381 numbers on the right depict the position of the amino acid in the particular sequence). (B)
1382 *In vitro* import of *Ng*GspD into isolated yeast mitochondria over a period of 16 min.
1383 Dissipation of the membrane potential (ΔΨ) by AVO mix abolished the import of matrix
1384 reporter protein (Su9-DHFR) bud did not affect the mitochondrial GspD; p – precursor of
1385 Su9-DHFR, m – mature form of the protein upon cleavage of the mitochondrial targeting
1386 sequence. (C) Structural model of *Go*GspD built by ProMod3 on the *Vibrio cholerae*
1387 GspD template. Top and side view of a cartoon and a transparent surface representation
1388 of the *Go*GspD pentadecamer model is shown in blue. The amphipathic helical loop
1389 (AHL), a signature of the secretin family, is highlighted and coloured according to the
1390 secondary structure with strands in magenta, helices in cyan and loops in light brown.
1391 The C-terminal GpsD residues are highlighted as spheres. The detailed view of the AHL
1392 region shows the essential residues V162 and F166 pointing towards the membrane
1393 surface. (D) *In vitro* translation and assembly of mitochondrial *Go*GspD into a high-
1394 molecular-weight complex; lipo – liposomes added, urea – liposome fraction after 2M
1395 urea treatment. (E) Y2H assay suggests the self- and mutual interaction of *Ng*GspD and
1396 *Ng*GspDN1.
1397
1398 **Fig. 5 Membrane pore formation of mitochondrial GspD.** (A) Expression of
1399 mitochondrial *Ng*GspD in bacteria quickly causes cell death upon induction. (B) Size
1400 exclusion chromatography of *Ng*GspD shows two peaks of putative GspD complexes
1401 (bottom) and SDS-PAGE of the corresponding fractions (top). (C) Single channel
1402 recording of the *Ng*GspD complex. The applied membrane potential was 15 mV. (D)
1403 Histogram of different recorded amplitudes during channel opening indicates multiple
1404 types of *Ng*GspD-formed pores in the membrane.
1405
1406 **Fig. 6 Structure and maturation of mitochondrial GspG**. (A) Domain architecture of
1407 the bacterial and the mitochondrial pseudopilin GspG (top). The arrow indicates the
1408 processing site of the bacterial GspG during protein maturation. MTS – mitochondria
1409 targeting sequence, + – polar anchor, TMD – transmembrane domain, ND – novel
1410 domain. (Bottom) Protein sequence alignment of the pseudopilin domains of
1411 mitochondrial and bacterial GspG proteins (in case two paralogues are present, only
1412 GspG1 is shown) (B) Homology modelling of *Go*GspG1. Top: pairwise alignment of
1413 protein sequences of *Go*GspG1 and *Klebisella oxytoca* PulG (the template used in model
1414 building). Regions of high sequence similarity are highlighted, including the hydrophobic
1415 segment (cyan), the α-β loop (magenta) and GspG signature loop with conserved Pro
1416 residues (green). Bottom: side and top views of the cartoon and transparent surface
1417 representation of *Go*GspG pilus model based on the pseudopilus cryo-EM
1418 reconstruction[47]. Proteins are coloured based on the secondary structure, with helix
1419 regions in cyan and loops in light brown. The regions of GspG1 sharing high similarity
1420 with PulG are highlighted with the same colour code as in the sequence alignment, with
1421 side chains shown in magenta and green. Inset: Detail of the structurally conserved loop
1422 regions. The novel domain (ND) specific to mitochondrial GspG proteins was omitted
1423 from the modelling. (C) Peptides specific to *Ng*GspG1 retrieved from the proteomic

1424 analysis of *N. gruberi* mitochondria. The Leu residue highlighted in blue indicates
1425 residue +1 following the processing site of bacterial GspG proteins.
1426
1427 **Fig. 7 The protein interactions of mitochondrial GspG.** (A) The soluble part of the
1428 pseudopilin domain was purified to homogeneity on and ran through a gel filtration
1429 column, which demonstrated the stable monomeric state of the protein. (B)
1430 Thermophoresis of NT-647-labelled protein showed specific self-interaction of the
1431 domain (top); plotting of the change in thermophoresis yielded a K_d of 216 ± 15.1 nm,
1432 concentration of the labelled GspG was 10 nM (bottom). (C) Positive interaction between
1433 the mitochondrial GspG protein and other mitochondrial T2SS subunits as determined by
1434 the BACTH assay. The error bars depict standard error of mean.
1435
1436 **Fig. 8 Proteins with the same phylogenetic profile as the originally identified**
1437 **mitochondrial Gsp homologues.** (A) Schematic domain representation of 23 proteins
1438 occurring in heteroloboseans, jakobids and malawimonads with the core T2SS subunits
1439 but not in other eukaryotes analyzed. Proteins with a functional link to the T2SS
1440 suggested by sequence homology are shown in blue, proteins representing novel
1441 paralogues within broader (super)families are shown in violet, and proteins without
1442 discernible homologues or with homologues only in prokaryotes are shown in pink. The
1443 presence of conserved protein domains or characteristic structural motifs is shown if
1444 detected in the given protein. Grey block – predicted transmembrane domain (see also
1445 Supplementary Fig. 11); "C H C H" – the presence of absolutely conserved cysteine and
1446 histidine residues (see also Supplementary Fig. 12) that may mediate binding of a
1447 prosthetic group; "HEXXH" and "EXXA" in Gcp16 indicate absolutely conserved motifs
1448 suggesting that the protein is a metallopeptidase of the gluzincin group (see text). The
1449 length of the rectangles corresponds to the relative size of the proteins. (B) Protein
1450 sequence alignment of Gcp12 proteins with highlighted conserved cysteine (black circles)
1451 and histidine (red circles) residues. (C) The expression of *Go*Gcp12 in *T. brucei* with the
1452 C-terminal V5 tag (green) showed partial co-localization with the mitochondrion (red).
1453
1454 **Fig. 9 The mitochondrial T2SS (miT2SS) as part of a hypothetical eukaryotic**
1455 **functional pathway connecting the mitochondrion and the peroxisome.** The scheme
1456 presents the most reasonable interpretation of the findings reported in this study, but
1457 further work is needed to test details of the working model. According to the model, a
1458 nucleus-encoded protein (green), possibly one of the newly identified Gcp proteins, is
1459 imported via the TOM complex into the mitochondrial inner membrane space, where it is
1460 modified by addition of a specific prosthetic group. After folding it becomes a substrate
1461 of the miT2SS machinery, is exported from the mitochondrion and finally reaches the
1462 peroxisome. The loading of the prosthetic group, the delivery to the peroxisome and
1463 possibly also the actual function of the protein in the peroxisome is assisted by specific
1464 subsets of other Gcp proteins. The hypothetical presence of Gcp proteins in specific
1465 (sub)compartments is depicted as a group of orange ovals. OMM – outer mitochondrial
1466 membrane, IMS – intermembrane space, IMM – inner mitochondrial membrane, MM –
1467 mitochondrial matrix
1468
1469

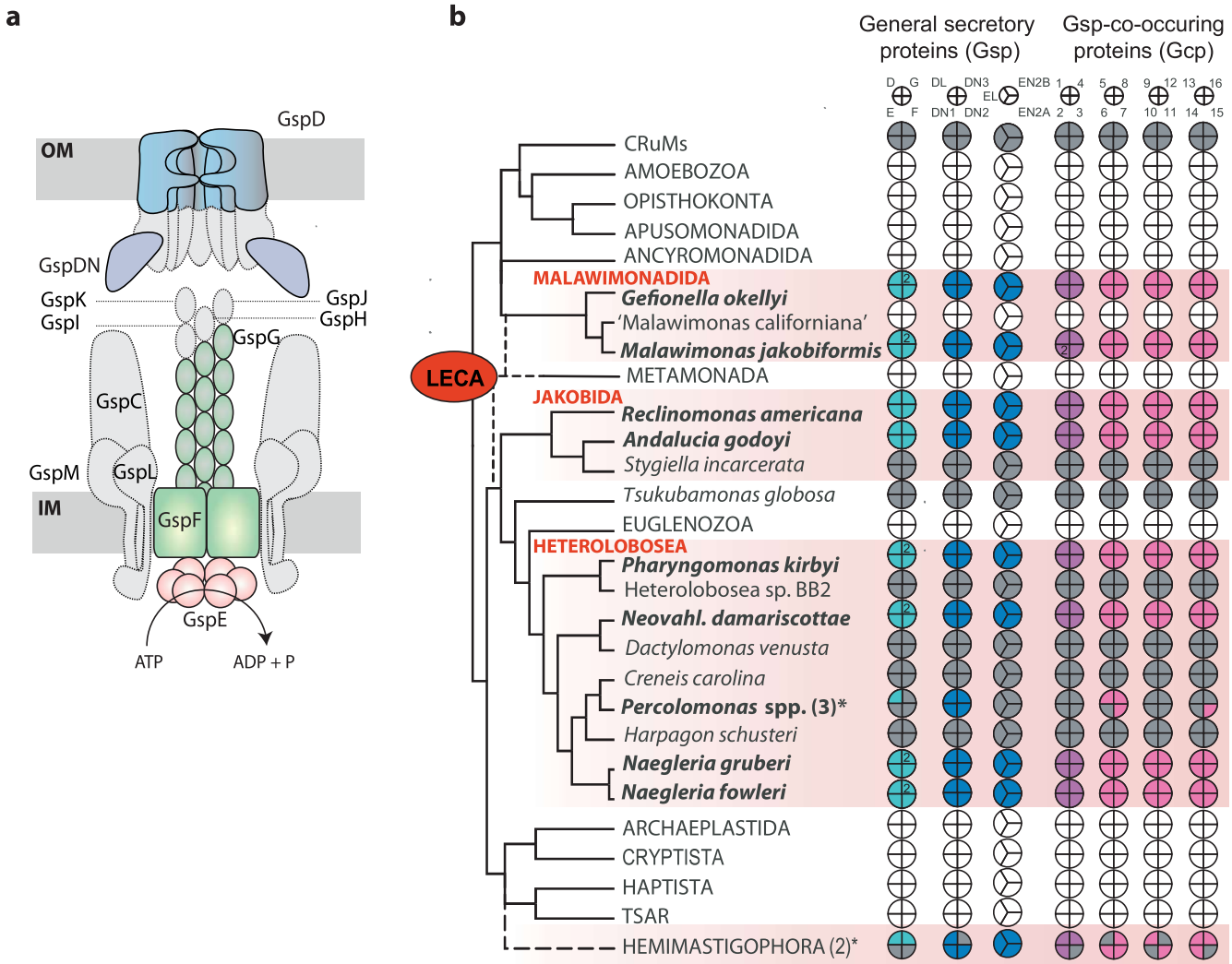
a
OM
GspD
GspDN
GspK
GspI
GspJ
GspH
GspG
GspC
GspM
GspL
IM
GspF
GspE
ATP
ADP + P
b
General secretory proteins (Gsp)
Gsp-co-occuring proteins (Gcp)
D G DL DN3 EN2B 1 4 5 8 9 12 13 16
E F DN1 DN2 EL EN2A 2 3 6 7 10 11 14 15
LECA
CRuMs
AMOEBOZOA
OPISTHOKONTA
APUSOMONADIDA
ANCYROMONADIDA
MALAWIMONADIDA
Gefionella okellyi
'Malawimonas californiana'
Malawimonas jakobiformis
METAMONADA
JAKOBIDA
Reclinomonas americana
Andalucia godoyi
Stygiella incarcerata
Tsukubamonas globosa
EUGLENOZOA
HETEROLOBOSEA
Pharyngomonas kirbyi
Heterolobosea sp. BB2
Neovahl. damariscottae
Dactylomonas venusta
Creneis carolina
Percolomonas spp. (3)*
Harpagon schusteri
Naegleria gruberi
Naegleria fowleri
ARCHAEPLASTIDA
CRYPTISTA
HAPTISTA
TSAR
HEMIMASTIGOPHORA (2)*

Figure 1

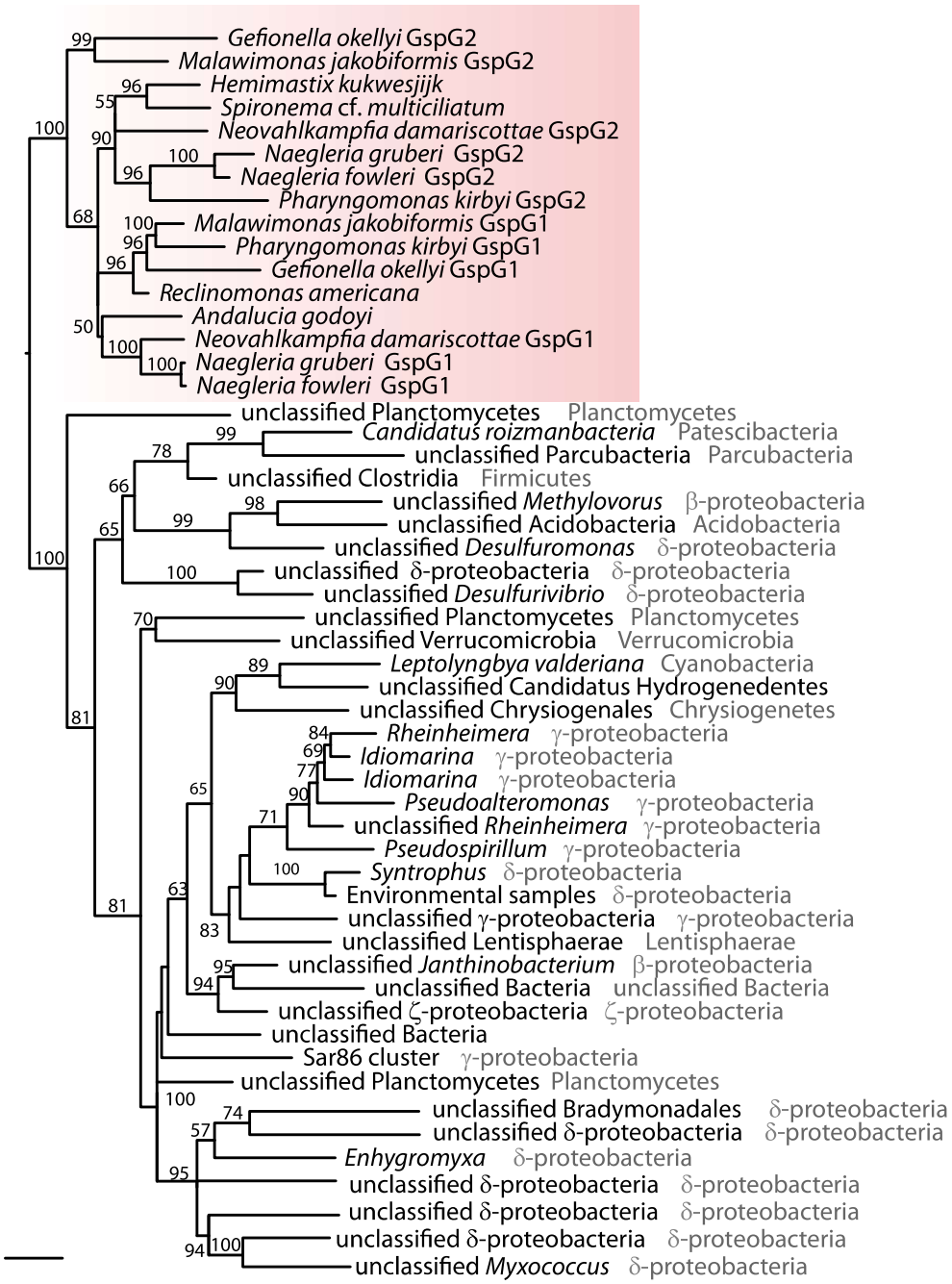
Gefionella okellyi GspG2
Malawimonas jakobiformis GspG2
Hemimastix kukwesijijk
Spironema cf. multiciliatum
Neovahlkampfia damariscottae GspG2
Naegleria gruberi GspG2
Naegleria fowleri GspG2
Pharyngomonas kirbyi GspG2
Malawimonas jakobiformis GspG1
Pharyngomonas kirbyi GspG1
Gefionella okellyi GspG1
Reclinomonas americana
Andalucia godoyi
Neovahlkampfia damariscottae GspG1
Naegleria gruberi GspG1
Naegleria fowleri GspG1
unclassified Planctomycetes Planctomycetes
Candidatus roizmanbacteria Patescibacteria
unclassified Parcubacteria Parcubacteria
unclassified Clostridia Firmicutes
unclassified Methylovorus β-proteobacteria
unclassified Acidobacteria Acidobacteria
unclassified Desulfuromonas δ-proteobacteria
unclassified δ-proteobacteria δ-proteobacteria
unclassified Desulfurivibrio δ-proteobacteria
unclassified Planctomycetes Planctomycetes
unclassified Verrucomicrobia Verrucomicrobia
Leptolyngbya valderiana Cyanobacteria
unclassified Candidatus Hydrogenedentes
unclassified Chrysiogenales Chrysiogenetes
Rheinheimera γ-proteobacteria
Idiomarina γ-proteobacteria
Idiomarina γ-proteobacteria
Pseudoalteromonas γ-proteobacteria
unclassified Rheinheimera γ-proteobacteria
Pseudospirillum γ-proteobacteria
Syntrophus δ-proteobacteria
Environmental samples δ-proteobacteria
unclassified γ-proteobacteria γ-proteobacteria
unclassified Lentisphaerae Lentisphaerae
unclassified Janthinobacterium β-proteobacteria
unclassified Bacteria unclassified Bacteria
unclassified ζ-proteobacteria ζ-proteobacteria
unclassified Bacteria
Sar86 cluster γ-proteobacteria
unclassified Planctomycetes Planctomycetes
unclassified Bradymonadales δ-proteobacteria
unclassified δ-proteobacteria δ-proteobacteria
Enhygromyxa δ-proteobacteria
unclassified δ-proteobacteria δ-proteobacteria
unclassified δ-proteobacteria δ-proteobacteria
unclassified δ-proteobacteria δ-proteobacteria
unclassified Myxococcus δ-proteobacteria

Figure 2

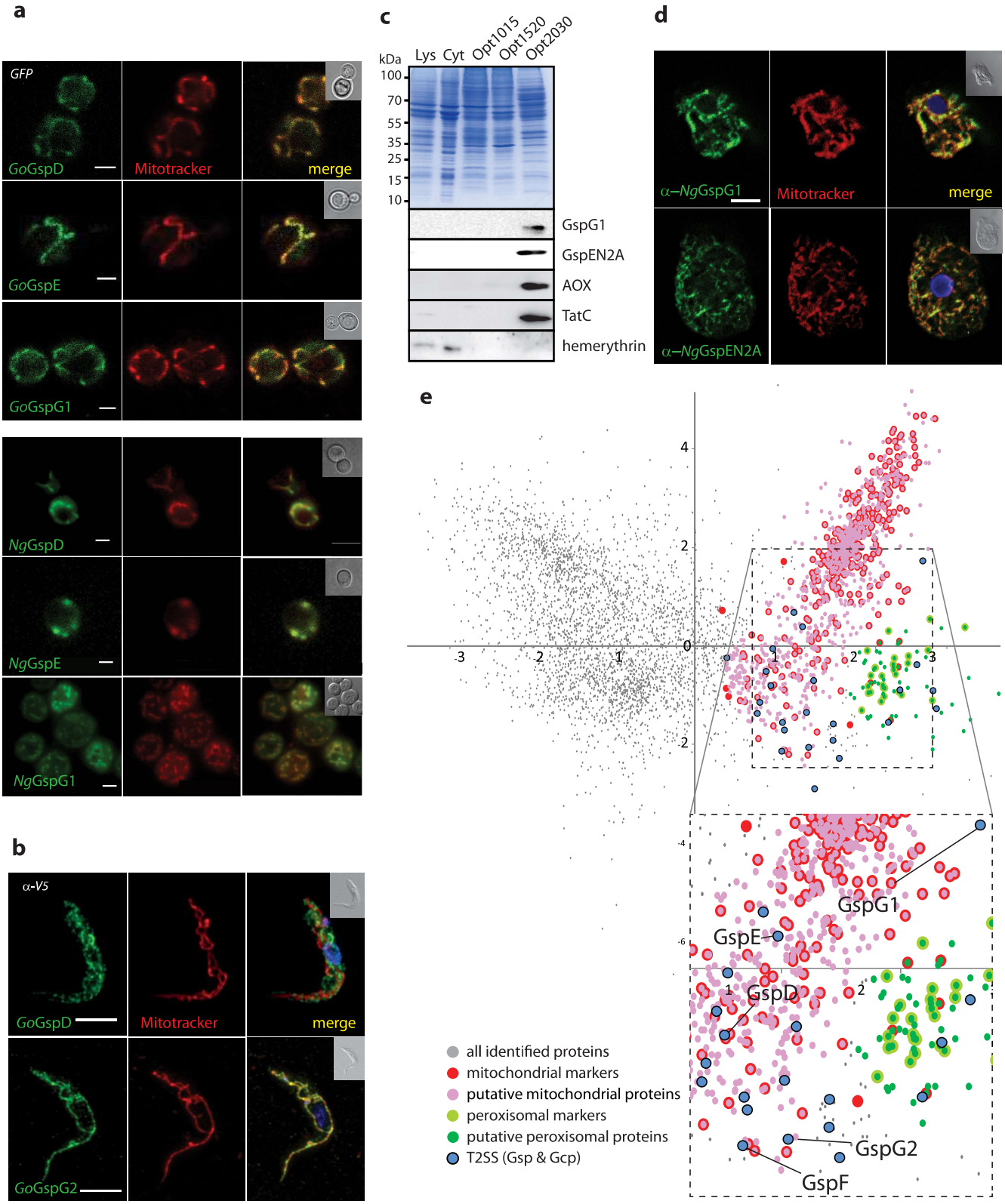
a
GFP
GoGspD
Mitotracker
merge
GoGspE
GoGspG1
NgGspD
NgGspE
NgGspG1
b
α-V5
GoGspD
Mitotracker
merge
GoGspG2
c
kDa
Lys
Cyt
Opt1015
Opt1520
Opt2030
100
70
55
35
25
15
10
GspG1
GspEN2A
AOX
TatC
hemerythrin
d
α–NgGspG1
Mitotracker
merge
α–NgGspEN2A
e
all identified proteins
mitochondrial markers
putative mitochondrial proteins
peroxisomal markers
putative peroxisomal proteins
T2SS (Gsp & Gcp)
GspG1
GspE
GspD
GspG2
GspF

Figure 3

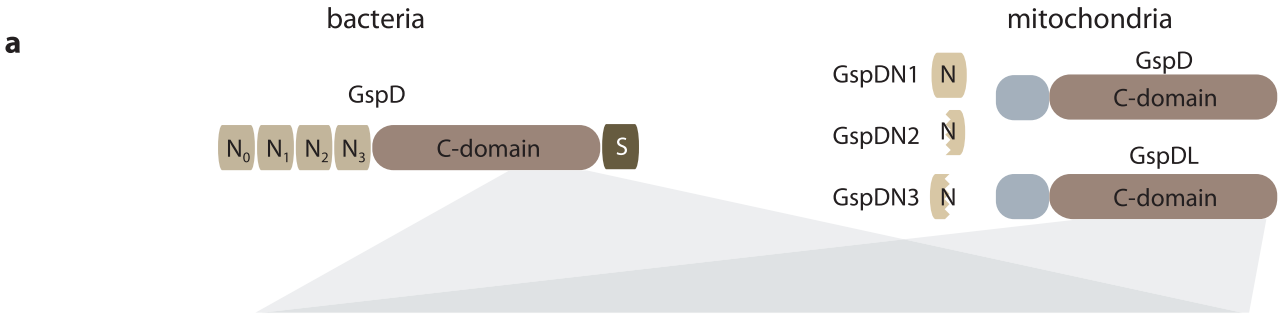


```
A. godoyi D          TQTAVRVRP-SDSQFLGSFALSTELRTVQSGP-LALIP--F-LKH---WFSRTE---------FVLVKSAILVFLTL------HVEPY 147
R. americana D       LQTAMLLKE-NVPSYAGSFALATELRRVRRSP-LSFIP--F-LER---FFSRHE---------FMLVKSAILVFITV------RTEAA 173
N. gruberi D         TSTNLLIKEFDKPHFVGSFSNSTELKTIRKSP-LSFIP--F-LSD---LFTRNE---------YMIVKSAILVFITA------SLKND 221
N. fowleri D         ASTNLLIRELNTPHFVGSFANSTELKAIRKSP-LSFLPFQF-LSQ---LFSRNE---------YMLVKSAILVFITA------SLDQQ 251
Neo. damariscottae D FQTNVLLKP-NQPTYVGAFSSSTELQTVKRSP-FSYLP--F-LRD---LFSRKE---------FILIKSAILVFITA------KYEDK 152
P. cosmopolitus WS D CQTQLMVQP-NEPTYVGAFAMSTDIRTVRQSPLRA-----L-WGW---LWDRTE---------YLKIKSALLVFVTC------RILKP 270
P. cosmopolitus AE-1 D VQTNMLLTP-NEPTFVGAFAVSQQLKTIKRSP-LSFLP--F-LKW---IFARTE---------YMLIKSAVLVFITA------RFSES 252
P. kirbyi D          VQTTVMLKE-NEPSFAGAFAASTELRTVKKSP-FSFLP--FKWGKA--LFSRTE---------FMLVKSAILVFIKCIPQRAFNVTET 206
M. jakobiformis D    LQTSVMLKE-NQATYVGAFAISNELKTIRRGP-LSYIP--L-IGD---LFRRDE---------FMRVKSAILVFVTC------RAERT 156
G. okellyi D         LQTSLMLKE-GQTTYAGSFALASELKTLKQGP-LSFLP--V-VGQ---LFSRDE---------FMLIKSAVLVFVTF------HKERS 189
H. kukwesjijk D      LQTTMMLKE-NQTTYVGALAVGTELRTVKRSP-LSYIP--F-LSR---LFTREE---------FMRVKSAILVFITA------RLQKL 200
E. coli T2SS         LKTTVLAND-GELIVLGGLMDDQAGESVAKVPLLGDIP--L-IGN---LFKSTA---------DKKEKRNLMVFIRP------TILRD 627
V. cholerae T2SS     LNTSVMVQD-GQMLVLGGLIDERALESESKVPLLGDIP--L-LGQ---LFRSTS---------SQVEKKNLMVFIKP------TIIRD 612
P. aeruginosa T2SS   IKSTILAEN-GQVIVIGGLIQDDVSQAESKVPLLGDIP--L-LGR---LFRSTK---------DTHTKRNLMVFLRP------TVVRD 606
N. meningitis T4P    LNTQAMVEN-GGTLIVGGIYEEDNGNTLTKVPLLGDIP--V-IGN---LFKTRG---------KKTDRRELLIFITP------RIMGT 754
M. xanthus T4P       ANTQVLVKD-GDTTVIGGIYVRRGATQVNSVPFLSRIP--V-LGL---LFKNNS---------ETDTRQELLIFITP------RILNR 894
S. enterica T3SS     ISTIARVPH-GKSLLVGGYTRDANTDTVQSIPFLGKLP--L-IGS---LFRYSSKNKSNVVRVFMIEPKEIVDPLTPDASESVNNILK 405
A. salmonicida T2SS  VKNAVLVKS-GETVVLGGLMDEQTKEEVSKVPLLGDIP--V-LGY---LFRSTS---------NTTSKRNLMVFIRP------TILRD 601
A. godoyi DL         --TELWLQD-GETVAVLGDGKEREFRTHYSPMYRRPFFSGW-IGRLL-QFLALDRLFGLHIDSHKKSRTRSVLLVTA------KLLPL 155
R. americana DL      --AELTLRD-GETAMLSGDSRSKSYRTHYSPEYRSSFFYSW-LGKLM-RLLWLDRLFGLHVDTVKHVRTRSYVFVTA------RILPD 154
N. gruberi DL        --AEVWLND-GETVVLSGDSRKKTYRTHYSPEYLRSFFFGW-VGRLI-RYLWMDRLFGLHVDTVKEVKTKNYIFVTA------QLLSE 188
N. fowleri DL        --AEVWLND-GETVVLNGDSRKKTYRTHYSPEYLRSFFFGW-VGRLI-RYLWLDRLFGLHVDTVKEVKTRNYIFVTT------QIIPE 189
Neo. damariscottae DL --TNVTLES-GRTVALQSQEREKVFRGRYWSGWKWYRMSGW-LKVLVYAFRW---LIGLNIDTVKKVKVSNMIYLTG------YVLPT 172
P. cosmopolitus WS DL --TEVWLND-GETVVLAADTRKKKYRTHYSPQFLRSFFFGW-IGRLL-RFLMLDRLFGLHVDTTKTVTTRNYIFVTA------HVLPS 172
P. cosmopolitus AE1 DL --AEVWLND-GETVVLSSDSRKKSYRTHYSPEYMRSFFFGW-IGRLL-RFFYLDRLFGLHVDTVKNVTIKNFIFVTA------HSLPI 196
P. kirbyi DL         --ASVWMND-GETVVLSADRKQRTYRTHYSPEFLRSFFYGW-LGRLL-RFFMLDRLFGFHMDTVKTVNKRSFVFVTA------HVLDT 142
M. jakobiformis DL   --AEVTLED-GETVVLAADSRVKTYRTHYSPFNRYSFS--W-LDRIL-RFLWLDRLLGLNIDSVKRIRTKSFIFVTA------HLLPH 120
G. okellyi DL        --AEVTLQD-GETVVLAADSRTKSYRTQYSPFNRYSFS--W-LDRLL-RFLWLDRLLGLHVDSVKHVRTKSFICVTA------HLLPS 226
S. cf multiciliatum DL --SEVMLND-GETAILSAHSRNRSYRLRYSP--IFSFVYGW-IRRFL-AFFWLDRLLGPQVDSVKTVKTKSFVMVSA------HILPA 137
```

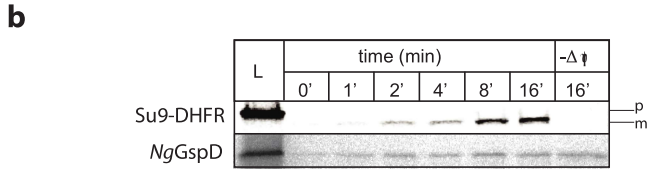

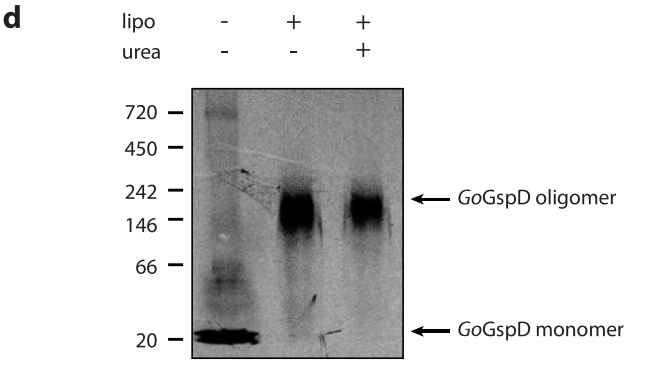

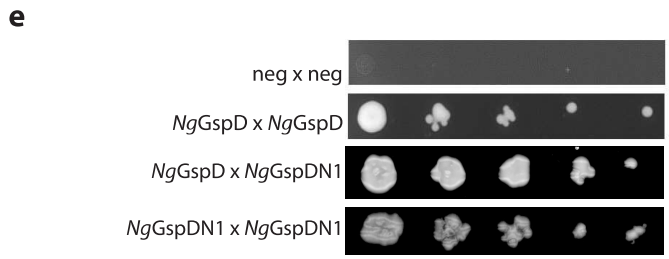

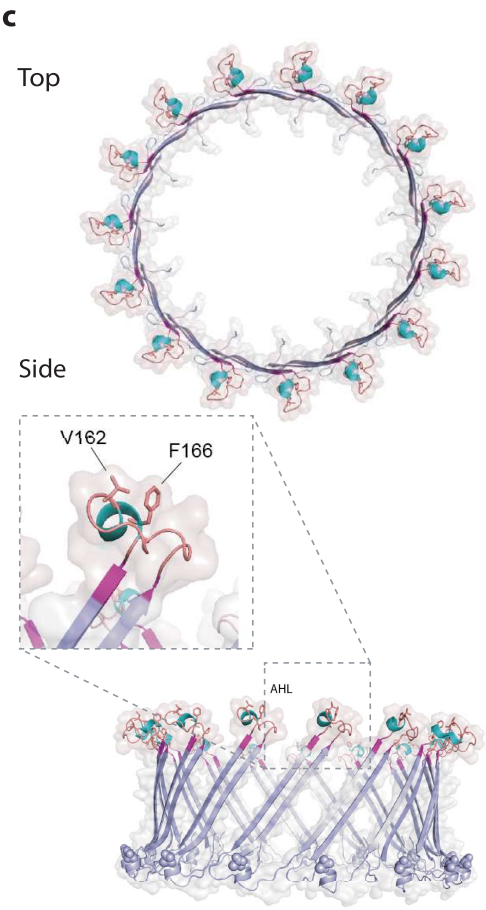

Figure 4

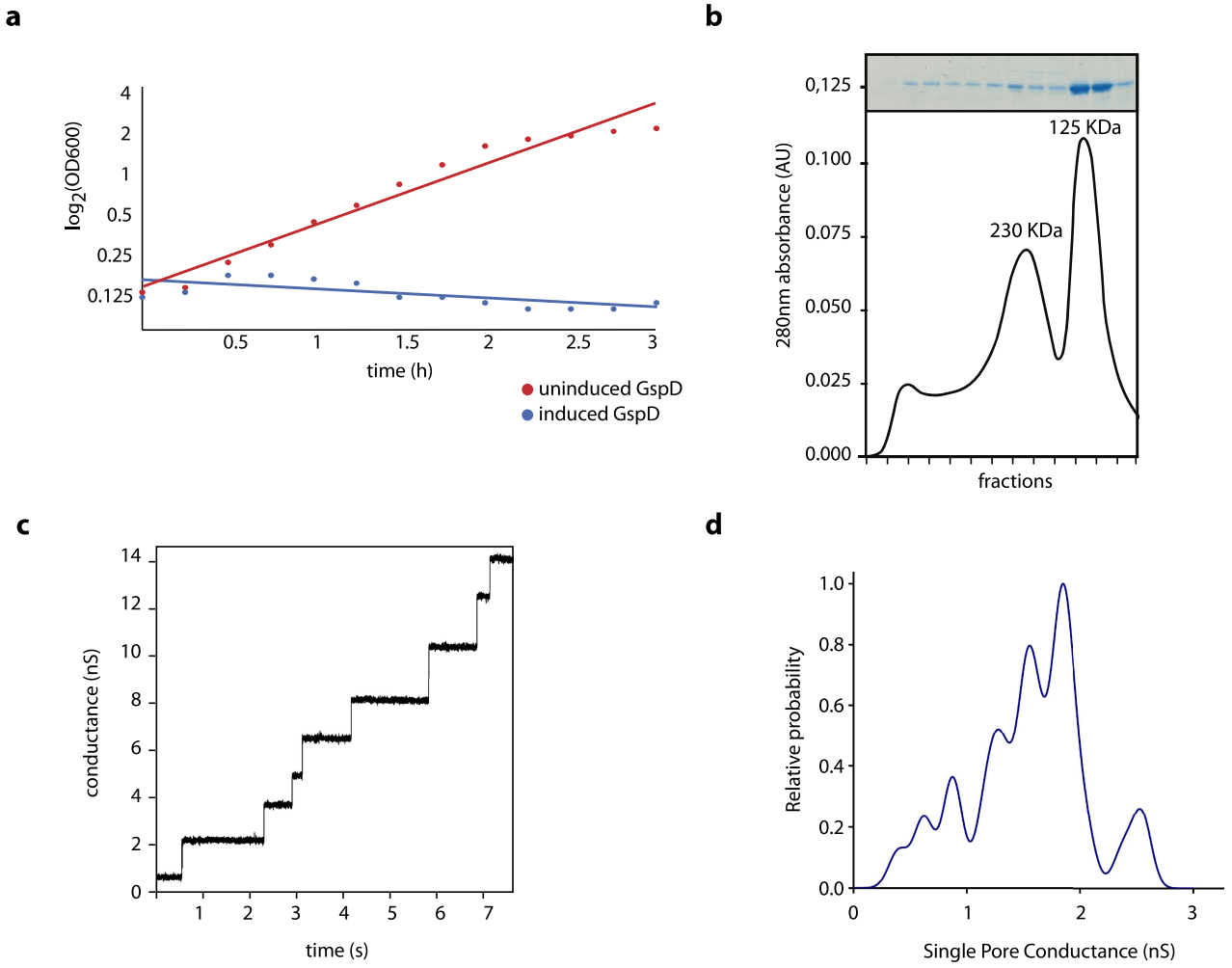
a
log2(OD600)
4
2
1
0.5
0.25
0.125
0.5
1
1.5
2
2.5
3
time (h)
uninduced GspD
induced GspD
b
0,125
0.100
0.075
0.050
0.025
0.000
280nm absorbance (AU)
125 KDa
230 KDa
fractions
c
conductance (nS)
14
12
10
8
6
4
2
0
1
2
3
4
5
6
7
time (s)
d
Relative probability
1.0
0.8
0.6
0.4
0.2
0.0
0
1
2
3
Single Pore Conductance (nS)

Figure 5

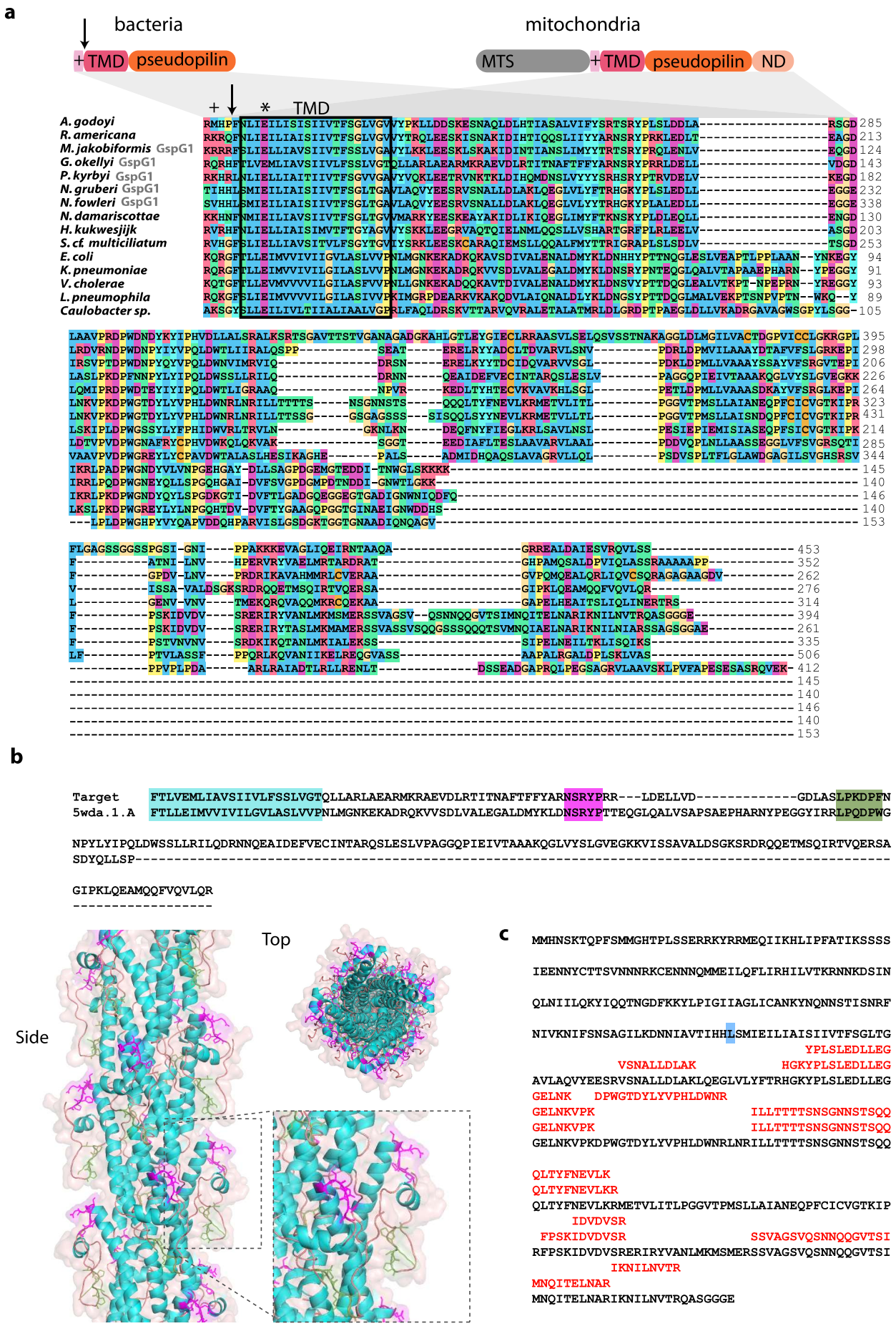
a
bacteria
mitochondria
+TMD pseudopilin
MTS +TMD pseudopilin ND
+ * TMD
A. godoyi
R. americana
M. jakobiformis GspG1
G. okellyi GspG1
P. kyrbyi GspG1
N. gruberi GspG1
N. fowleri GspG1
N. damariscottae
H. kukwesjijk
S. cf. multiciliatum
E. coli
K. pneumoniae
V. cholerae
L. pneumophila
Caulobacter sp.
b
Target
5wda.1.A
Top
Side
c

Figure 6

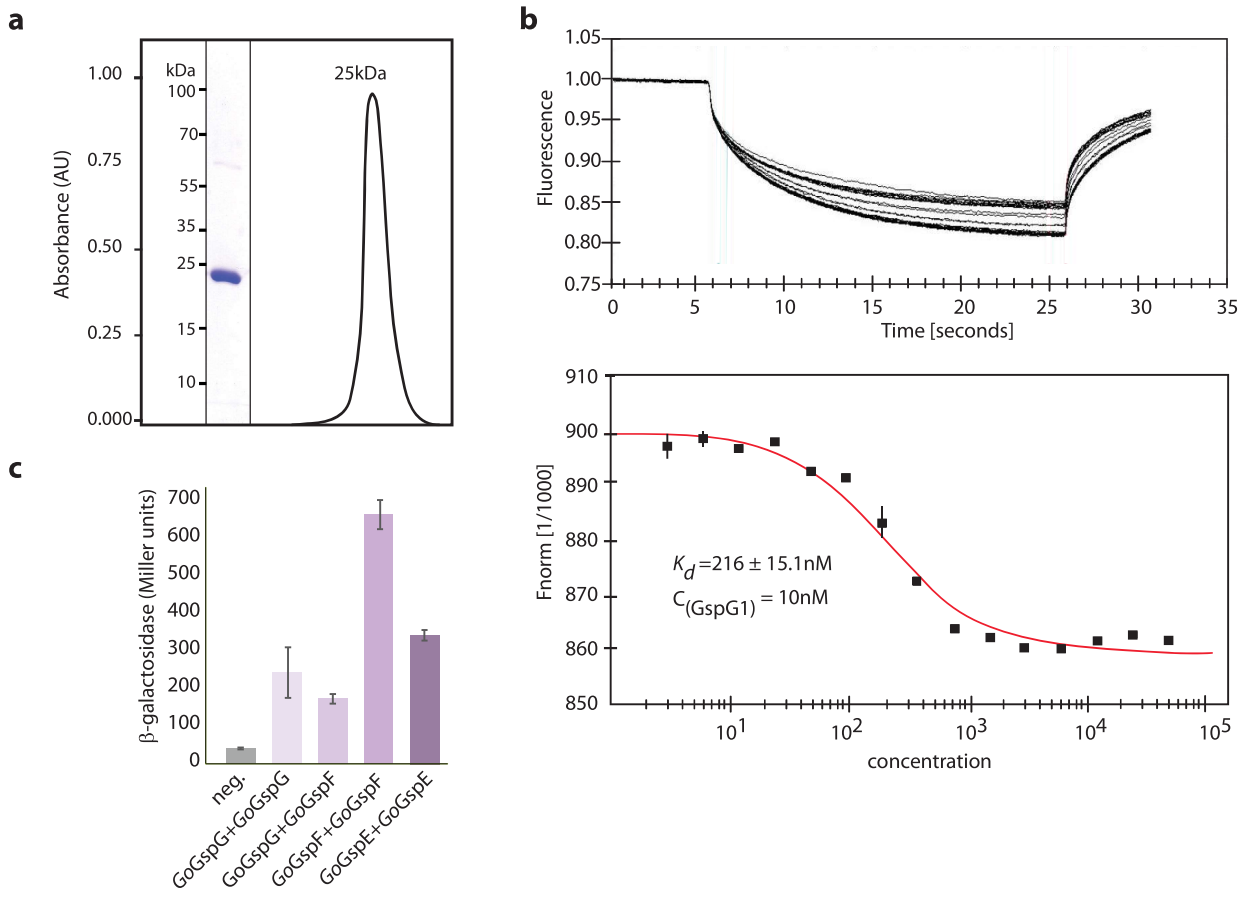
a
kDa
100
70
55
35
25
15
10
25kDa
Absorbance (AU)
1.00
0.75
0.50
0.25
0.000
b
Fluorescence
1.05
1.00
0.95
0.90
0.85
0.80
0.75
0
5
10
15
20
25
30
35
Time [seconds]
Fnorm [1/1000]
910
900
890
880
870
860
850
K_d=216 ± 15.1nM
$C_{(GspG1)}$ = 10nM
10^1
10^2
10^3
10^4
10^5
concentration
c
β-galactosidase (Miller units)
700
600
500
400
300
200
100
0
neg.
GoGspG+GoGspG
GoGspG+GoGspF
GoGspF+GoGspF
GoGspE+GoGspE

Figure 7

a

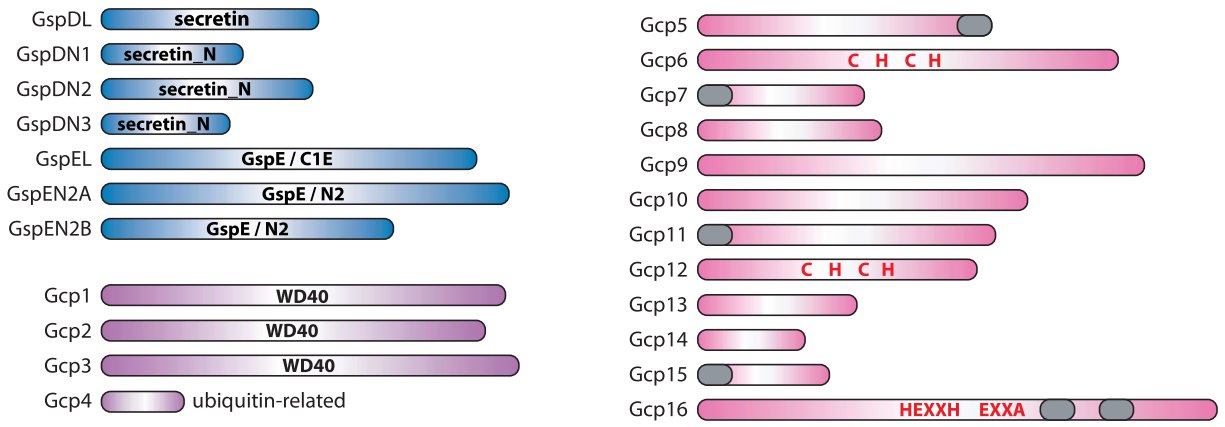
GspDL
secretin
GspDN1
secretin_N
GspDN2
secretin_N
GspDN3
secretin_N
GspEL
GspE / C1E
GspEN2A
GspE / N2
GspEN2B
GspE / N2
Gcp1
WD40
Gcp2
WD40
Gcp3
WD40
Gcp4
ubiquitin-related
Gcp5
Gcp6
C H C H
Gcp7
Gcp8
Gcp9
Gcp10
Gcp11
Gcp12
C H C H
Gcp13
Gcp14
Gcp15
Gcp16
HEXXH EXXA

b

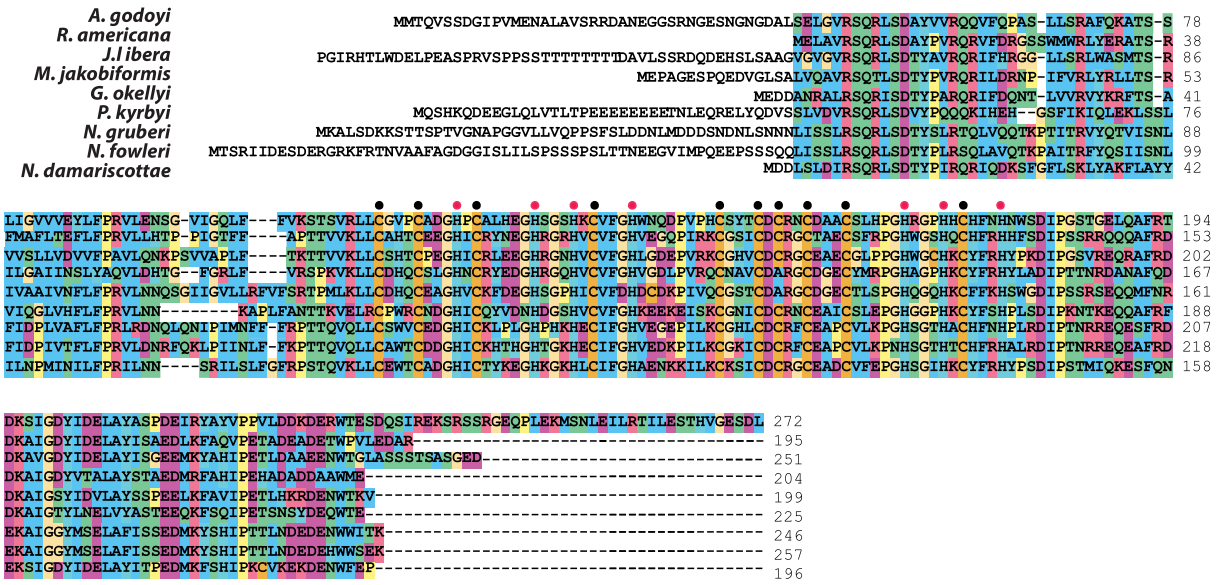
A. godoyi
R. americana
J.l ibera
M. jakobiformis
G. okellyi
P. kyrbyi
N. gruberi
N. fowleri
N. damariscottae

c

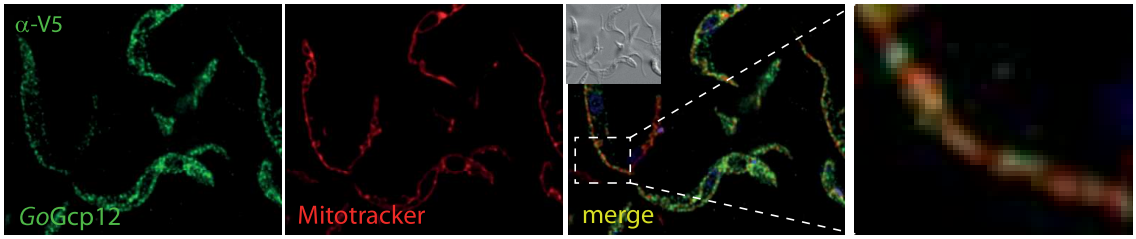
α-V5
GoGcp12
Mitotracker
merge

Figure 8

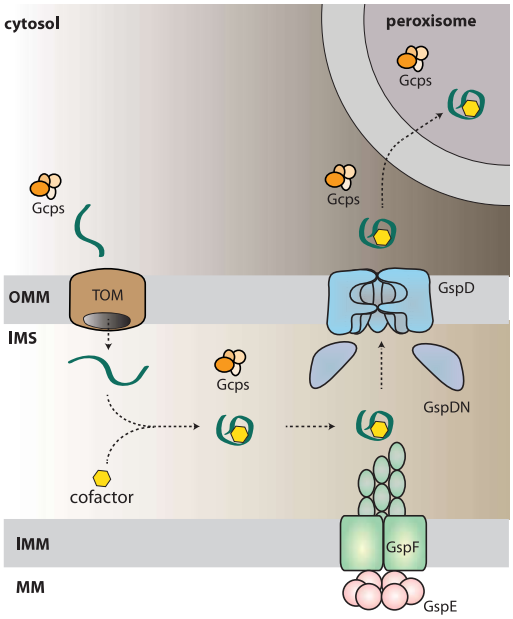
cytosol
peroxisome
Gcps
Gcps
Gcps
OMM
TOM
GspD
IMS
Gcps
GspDN
cofactor
IMM
GspF
MM
GspE

Figure 9